

8

Magneto-optic Studies on II-VI Semiconductor Quantum Dots in Glass Composites and on Rare Earth Containing Glasses: Non-Linear Faraday Effect and Nano-scale In-homogeneities

John Schroeder^{1*}, Joseph H. Kratzer²

¹Rensselaer Polytechnic Institute, Department of Physics, Applied Physics and Astronomy, 110 8th St., Troy, NY 12180-3590 USA

²P.O. Box 229, Bennington, VT 05201 USA

Outline:

Introduction.....	191
Theoretical Background and Aspects	192
<i>Faraday Rotation</i> **	192
<i>Preliminary Concepts</i>	192
<i>Faraday Rotation: A Classical Derivation and a Quantum Mechanical Treatment</i>	193
<i>Intermediate Range Order in Glasses: Boson Peaks and Nanoscale Inhomogeneities</i>	199
<i>The relations of the correlation volume to the distribution of relaxation times</i>	199
<i>The Boson Peak and the Density of Vibrational States and Intermediate Range Order (IRO)</i>	201
<i>Summary Comments on Boson Peaks and Nanoscale Inhomogeneities</i>	203
Experimental Techniques	203
Results	206
Discussions	214
Conclusions	221
References	224

Introduction

Magneto-optic effects in II-VI semiconductor nano-crystals embedded in borosilicate glass have been investigated in a number of preliminary studies up until now. Considerable interest has existed in the Faraday effect in metals and semiconductors, due to the information which could be obtained, relating to elucidation of electronic states, effective masses, and to further the understanding of the theory of solids in a magnetic field. References [1-8] represent a few of many papers concerned with semiconductors in this context.

Following the bulk semiconductors came diluted magnetic semiconductors of the type, $A^{II}_{1-x}Mn_xB^{VI}$, where A is the type II element and B is a type VI element and Mn is the substitutional magnetic ion. A review of these types of materials is given by Furdyna [9, 10] in which giant Faraday rotation is discussed. The step in proceeding from bulk materials to nanocrystals with respect to measurement of enhanced Faraday rotation (but not a non-linearity) has been documented by a number of authors [10-15]. Here three dimensionally confined diluted magnetic semiconductor clusters of nanocrystalline size were synthesized inside a glass matrix. Wang, et.al [12] observed the effect of size quantization on the exciton energy. They studied the diluted magnetic semiconductors of the type $A^{II}_{1-x}Mn_xB^{VI}$ with the magnetic ion being Mn^{++} . This exchange interaction constitutes an interplay between the semiconductor and magnetism giving a large Faraday rotation in three dimensionally confined clusters [12]. Nikitin, et. al [16] prepared $Cd_{1-x}Mn_xTe$ nanocrystals embedded in an SiO_2 matrix. A study of the Faraday Effect in these semi-magnetic semiconductor nanocrystals has revealed large enhancements of the effect, when compared to the bulk $Cd_{1-x}Mn_xTe$ crystal. Additional evidence for a Faraday Effect enhancement has been predicted [17, 18].

We have studied both paramagnetic and diamagnetic materials with respect to Faraday rotation measurements [19]. In our work with paramagnetic rare earth ions in glasses, we find that Terbium oxide provides the strongest Faraday rotation, followed by Dysprosium oxide and Praseodymium oxide. The particular rare earth ion and its concentration determine the magnitude of the Faraday rotation, while the host glass is relatively unimportant. For applications requiring large Faraday rotation (or large Verdet constants) dilute magnetic semiconductors become rather interesting. Preliminary work on nanocrystal CdS-glass composites have also been carried out by us. We determined that their Verdet constants are at least one to two orders of magnitude greater than SiO_2 glass. Also, there is a significant effect of quantum dot size and interatomic lattice spacing on the magnitude of Faraday rotation. There appears to be an effect of homogeneity of quantum dot size on the magnitude and nonlinearity of Faraday rotation, as well. We carried out Faraday rotation measurements on three dimensionally confined CdS, CdSe and CdTe semiconductor nanocrystals in a glass matrix, where particle size and distributions were carefully controlled. We have a wealth of experience in preparing both nanocrystalline semiconductors in glass composites with specified particle sizes and relatively small size distribution [20-23]. Low frequency Raman measurements, photoluminescence, x-ray diffraction and TEM analysis were employed to determine the particle size of our samples [24]. Even at room temperature, the II-VI semiconductor nanocrystals in a glass matrix have demonstrated unusual behavior of the Faraday Effect.

The rare earth containing glasses also showed a non-linearity in the Faraday rotation as function of magnetic field strength. However, Faraday rotation data for a single crystal NaCl sample exhibited no kinks up to 2.57 Tesla. Various mechanisms will be put forth and evaluated as to the feasibility of using these processes to explain the observed effects. We consider Landau levels, resonance effects, shape and piezo-electric effects, electron-spin correlation for the quantum dot composites; and intermediate range order (IRO) for the rare earth containing glass matrix itself and try to interpret how each of these mechanisms may or may not have an effect on the Faraday rotation behavior.

Theoretical Background and Aspects

Faraday Rotation **

Preliminary Concepts

Faraday rotation occurs when plane polarized light is passed through matter (a sample) parallel to the direction of an applied magnetic field. The linearly polarized light is a superposition of two circular polarizations, one rotating clockwise and the other counterclockwise when viewed along the direction of propagation. The application of a magnetic field removes the degeneracy of the resonant frequencies for the two circular polarizations. This results in a difference between their indices of refraction. As a result, one circular polarization will more rapidly pass through the material. When both polarizations emerge from the far end of the sample the recombined plane wave will have its plane of polarization rotated with respect to that of the incident light. More detailed explanations of Faraday rotation are given in the literature [19,25-33]. Faraday rotation is also closely related to dispersion theory [32] and the Zeeman effect [34,35].

The classic equation for Faraday rotation is $\Theta = V l B$

where l is the length of the sample and B the strength of the magnetic field. The constant of proportionality, V , is called the Verdet constant.

** “Actually, this discovery of Faraday (1845) was one of the important contributions to the electromagnetic theory of light since it was a connection between light and magnetism” [32].

For paramagnetic material the Verdet constant is given by the equation [34]

$$V_{\text{para}} = 4 \pi^2 \omega^2 \frac{\chi_m}{g \beta c h} \sum_{ij} \frac{C_{ij}}{(\omega^2 - \omega_{ij}^2)}$$

where g is the Lande` factor; β is the Bohr magneton; c the speed of light; h Planck’s constant and ω the angular frequency of the light. The terms C_{ij} and ω_{ij} are measures of the transition probability and energy splitting between the ground state and excited states, respectively. The term χ_m is the d.c. magnetic susceptibility of the sample which is given by the Curie-Weiss law.

For diamagnetic materials the frequency dependence of the Verdet constant derived from a quantum mechanical expression has the form [35]

$$V_{\text{dia}} = 4 \pi N \omega^2 \sum_{ij} \frac{C_{ij}}{(\omega^2 - \omega_{ij}^2)^2}$$

where C_{ij} is a function of the transition moments between the ground state and excited states. ω is the light frequency; ω_{ij} is the frequency difference of the ground and excited states; and N is the number of atoms per unit volume. The Verdet constant of diamagnetic materials is usually temperature independent.

For the non-linear Faraday effects Yu and Osborn [36] extended the theory of the Faraday Effect to treat non-linear terms in the electric field. A Verdet constant proportional to the light intensity was derived. Here, using a two energy level, the rotation of a non-uniform laser beam would be dependent on the beam intensity profile Perlin [37] formulated the theory for non-linear optical polarization

effects in quantum dot materials. He calculated the amplitude and dispersion relation of the cubic susceptibility tensor components and their combinations responsible for the Kerr and Faraday optical effects. It is shown that the susceptibilities increase smoothly in amplitude below the two-photon absorption threshold while remaining negative. Above the threshold, the susceptibilities exhibit sharp maxima associated with two-photon resonances.

Faraday Rotation: A Classical Derivation and a Quantum Mechanical Treatment

The following treatment comprises a review of Faraday rotation from the classical viewpoint followed by a quantum mechanical treatment [38]. Faraday discovered that the plane of polarized light passing through lead borate glass was altered when passing through the poles of an electromagnet. This rotation, a general property of matter is of the form,

$$\theta = VIB \quad (8.1)$$

Where V is the Verdet constant, l is the length of material through which light travels, and B is the magnetic field, in the direction of the light. This effect arises as a consequence of the different indices of refraction for right and left circularly polarized light (n_+ vs. n_-). In reality, plane polarized light passing through transparent materials exhibits not only a change in the direction of polarization, but also some ellipticity. The rotation of light in a magnetic field, magneto-optic rotation (MOR) is therefore to be distinguished from magnetic circular dichroism (MCD), which arises from the differential absorption of right and left circularly polarized light, associated with their different absorption coefficients (k_+ vs. k_-). Note: For more background and additional specific information and calculations regarding the Faraday Effect, and the calculations which follow see references [17-18, 28-35, 38]

Then, with ϕ as the angle of ellipticity, we have,

$$\theta = \frac{\omega}{2c} (n_- - n_+) \quad (8.2)$$

$$\phi = \frac{\omega}{2c} (k_- - k_+) \quad (8.3)$$

Now, before discussing the mechanism of MOR on a quantum mechanical basis, it will be discussed from a classical standpoint.

Then, we begin with the equation of motion of a valence electron,

$$m \frac{d^2 \mathbf{r}}{dt^2} = -e\mathbf{E} - e\mathbf{V} \times \mathbf{B} - m\omega_0^2 \mathbf{r} \quad (8.4)$$

with $\mathbf{P} = -Ne\mathbf{r}$ \mathbf{P} as the polarization vector, and $\omega_0 = \sqrt{\kappa/m}$, where κ is the spring constant to the fixed atomic site, for the electron. The equation for \mathbf{P} is then,

$$-\frac{m}{Ne} \frac{d^2 \mathbf{P}}{dt^2} = -e\mathbf{E} - e \left(-\frac{1}{Ne} \frac{d\mathbf{P}}{dt} \right) \times \mathbf{B} + \frac{m\omega_0^2}{Ne} \mathbf{P} \quad (8.5)$$

As $\mathbf{E}, \mathbf{P} \propto e^{i\omega t}$, $\frac{d}{dt} = i\omega$, then substituting into the above, we have,

$$\frac{m\omega^2}{Ne} \mathbf{P} = -e\mathbf{E} - \frac{i\omega \mathbf{B} \times \mathbf{P}}{Ne} + \frac{m\omega_0^2}{Ne} \mathbf{P} \quad (8.6)$$

$$\mathbf{E} = \frac{\omega_0^2 - \omega^2}{\varepsilon_0 \omega_p^2} \mathbf{P} + \frac{i\omega}{Ne} \mathbf{B} \times \mathbf{P} \quad (8.7)$$

with $\omega_p^2 = \frac{Ne^2}{m\varepsilon_0}$. Now, $\mathbf{B} = (0,0,B)$. Then,

$$\begin{pmatrix} E_x \\ E_y \\ E_z \end{pmatrix} = \begin{pmatrix} \frac{\omega_0^2 - \omega^2}{\varepsilon_0 \omega_p^2} & \frac{i\omega}{Ne} B & 0 \\ -\frac{i\omega}{Ne} B & \frac{\omega_0^2 - \omega^2}{\varepsilon_0 \omega_p^2} & 0 \\ 0 & 0 & \frac{\omega_0^2 - \omega^2}{\varepsilon_0 \omega_p^2} \end{pmatrix} \begin{pmatrix} P_x \\ P_y \\ P_z \end{pmatrix} \quad (8.8)$$

Then, with Maxwell's equations in a vacuum, and with $\mathbf{B} = \mu \mathbf{H}$, $\mathbf{D} = \mathbf{E} + 4\pi \mathbf{P}$ we have,

$$\mu_0 \varepsilon_0 \ddot{\mathbf{E}} - \nabla^2 \mathbf{E} = \frac{1}{\varepsilon_0} \nabla (\nabla \cdot \mathbf{P}) - \mu_0 \ddot{\mathbf{P}} \quad (8.9)$$

Then, with $\mathbf{E} = E_0 e^{i(\omega t - \mathbf{k} \cdot \mathbf{r})}$, $\mathbf{D} = \varepsilon_0 \mathbf{E} + \mathbf{P}$ we have $\partial^2 / \partial t^2 = -\omega^2$, $\nabla^2 \mathbf{E} = -k^2 \mathbf{E}$. And,

$$\nabla \cdot \mathbf{P} = -i\mathbf{k} \cdot \mathbf{P} = -ikP_z, \quad \nabla (\nabla \cdot \mathbf{P}) = -k^2 P_z \mathbf{e}_z \quad (8.10)$$

where $\mathbf{k} = k\mathbf{e}_z$. Then,

$$\varepsilon_0 (k^2 c^2 - \omega^2) \mathbf{E} = -k^2 c^2 P_z \mathbf{e}_z + \omega^2 \mathbf{P} \quad (8.11)$$

As $\mu_0 \varepsilon_0 = c^2$, and $1 + \chi = \frac{k^2 c^2}{\omega^2}$, $\chi = \frac{k^2 c^2}{\omega^2} - 1$, we have, $\varepsilon_0 \chi \mathbf{E} = P_x \mathbf{e}_x + P_y \mathbf{e}_y + \chi P_z \mathbf{e}_z$

$$\mathbf{E} = \frac{1}{\varepsilon_0 \chi} (P_x \mathbf{e}_x + P_y \mathbf{e}_y) - \frac{1}{\varepsilon_0} P_z \mathbf{e}_z \quad \text{and,}$$

$$\begin{pmatrix} E_x \\ E_y \\ E_z \end{pmatrix} = \frac{1}{\varepsilon_0 \chi} \begin{pmatrix} 1 & 0 & 0 \\ 0 & 1 & 0 \\ 0 & 0 & -\chi \end{pmatrix} \begin{pmatrix} P_x \\ P_y \\ P_z \end{pmatrix} \quad (8.12)$$

And, subtracting (8.12) from (8.08) we have,

$$\begin{pmatrix} \frac{\omega_0^2 - \omega^2}{\varepsilon_0 \omega_p^2} - \frac{1}{\varepsilon_0 \chi} & \frac{i\omega}{Ne} B & 0 \\ -\frac{i\omega}{Ne} B & \frac{\omega_0^2 - \omega^2}{\varepsilon_0 \omega_p^2} - \frac{1}{\varepsilon_0 \chi} & 0 \\ 0 & 0 & \frac{\omega_0^2 - \omega^2}{\varepsilon_0 \omega_p^2} + \frac{1}{\varepsilon_0} \end{pmatrix} \begin{pmatrix} P_x \\ P_y \\ P_z \end{pmatrix} = 0 \quad (8.13)$$

As the (3,3) term above, $\frac{\omega_0^2 - \omega^2}{\varepsilon_0 \omega_p^2} + \frac{1}{\varepsilon_0} \neq 0$, $P_z, E_z = 0$, meaning incident waves will remain plane waves. Also given the fact that non-vanishing solutions to the matrix necessitates that the determinant be zero, from (8.13) we have,

$$\frac{\omega_0^2 - \omega^2}{\varepsilon_0 \omega_p^2} - \frac{1}{\varepsilon_0 \chi_{\pm}} = \pm \frac{\omega B}{Ne} \quad (8.14)$$

Then, solving for χ_{\pm} and rearranging terms, we have,

$$n_{\pm} = \frac{ck_{\pm}}{\omega} = \sqrt{1 + \chi_{\pm}} = \sqrt{1 + \frac{Ne\omega_p^2}{Ne(\omega_0^2 - \omega^2) \mp \varepsilon_0 \omega_p^2 \omega B}} \quad (8.15)$$

Also, looking at Equation (8.13), corresponding to we n_{\pm} have, $\frac{\omega B}{Ne} P_z = \pm \frac{i\omega B}{Ne} P_y$, $P_y = \pm i P_x$. Then,

$$P_{\pm} = C_{\pm} \begin{pmatrix} 1 \\ \pm i \\ 0 \end{pmatrix}, \quad E_{\pm} = \frac{C_{\pm}}{\varepsilon_0 \chi_{\pm}} \begin{pmatrix} 1 \\ \pm i \\ 0 \end{pmatrix} \quad (8.16)$$

And, rearranging terms in Equation 8.15, and using $\omega_p^2 = \frac{Ne^2}{m\varepsilon_0}$ we have,

$$n_{\pm} = \sqrt{1 + \frac{Ne/m\varepsilon_0}{(\omega_0^2 - \omega^2) \mp \omega_c \omega}} \quad (8.17)$$

where ω_c is the cyclotron frequency. This shows that, from a classical standpoint, the alteration of the indices of refraction for right and left-circularly polarized light are influenced by an analog of the cyclotron frequency, and thence the magnetic field.

Next, we proceed with the quantum mechanical explanation of Faraday rotation.

Here, we are concerned only with MOR, and therefore will consider only equation (8.2). Then, we note that [17],

$$\mathbf{D} = \mathbf{E} + 4\pi \sum_a N_a m^a \quad \mathbf{B} = \mathbf{H}' + 4\pi \sum_a N_a \mu^a \quad (8.18)$$

where N_a is the number of molecules in state a , and the electric and magnetic moments are m and μ respectively. Much of the following follows from reference [17]. Then, to first order, the components of the complex induced moment vectors are ($\alpha = x, y, z$),

$$m_\alpha = \alpha_{\alpha\beta} E_\beta + \beta_{\alpha\beta} H'_\beta \quad \mu_\alpha = \gamma_{\alpha\beta} E_\beta + \chi_{\alpha\beta} H'_\beta \quad (8.19)$$

with α, χ the electric and magnetic polarizability tensors, respectively. These tensors are functions of the static magnetic field, \mathbf{H} , with $\alpha_{\alpha\beta} = \alpha_{\alpha\beta}^0 + \alpha_{\alpha\beta\gamma}^{(1)} H_\gamma + \dots$. In an isotropic material, such as semiconductor quantum dots, the isotropic parts of the tensors may be used.

Then, $\alpha_{\alpha\beta}^{(0)} = \alpha_{(0)} \delta_{\alpha\beta}$, $\alpha_{\alpha\beta\gamma}^{(1)} = \alpha_{(1)} \varepsilon_{\alpha\beta\gamma}$, with $\alpha_{(0)} = \frac{1}{3} \alpha_{\alpha\beta}^{(0)} \delta_{\alpha\beta} = \frac{1}{3} \alpha_{\beta\beta}^{(0)}$, $\alpha_{(1)} = \frac{1}{6} \alpha_{\alpha\beta\gamma}^{(1)} \varepsilon_{\alpha\beta\gamma}$ and with $\delta_{\alpha\beta}$ as the Kroenecker delta function and with $\varepsilon_{\alpha\beta\gamma}$ as the Levi-Civita symbol. Then, we have,

$$m = \alpha_{(0)} \mathbf{E} + \beta_{(0)} \mathbf{H}' + \alpha_{(1)} (\mathbf{E} \times \mathbf{H}') + \alpha_{(1)} (\mathbf{E} \times \mathbf{H}) + \beta_{(1)} (\mathbf{H}' \times \mathbf{H}) \quad (8.20)$$

$$\mu = \gamma_{(0)} \mathbf{E} + \chi_{(0)} \mathbf{H}' + \gamma_{(1)} (\mathbf{E} \times \mathbf{H}) + \chi_{(1)} (\mathbf{H}' \times \mathbf{H}) \quad (8.21)$$

It should be noted that the magneto-optic rotation contains $\theta = VH + \text{terms in } H^3, H^5, \text{ etc.}$ The reason for this is the nature of \mathbf{H} as a pseudo-vector which, unlike \mathbf{E} , does not change signs under change from a right to a left-handed frame. Since on reflection, right circularly polarized light is transformed into left circularly polarized light, etc., natural optic rotation is canceled upon reflection. However, MOR is not, as the sign of the constant \mathbf{H} , \mathbf{H}_z , e.g., is reversed upon reflection. Thus, MOR in isotropic materials is an odd function of \mathbf{H} .

Then, using the expression for the electric field vector,

$$\mathbf{E}_\pm = \mathbf{E}^{(0)} \exp[i\omega(t - n_\pm z / c)](i \mp 1) \quad (8.22)$$

along with Eqs. (8.5) and Maxwell's equations for light in media, we have [18]

$$\begin{aligned} n_\pm = 1 + \pi \sum_a N_a \{ & \alpha_{xx}^a + \alpha_{yy}^a \} \pm i(\alpha_{xy}^a - \alpha_{yx}^a) + (\chi_{xx}^a + \chi_{yy}^a) \pm i(\chi_{xy}^a - \chi_{yx}^a) \\ & \mp i(\beta_{xx}^a + \beta_{yy}^a) + (\beta_{xy}^a - \beta_{yx}^a) \pm i(\gamma_{xx}^a + \gamma_{yy}^a) - (\gamma_{xy}^a - \gamma_{yx}^a) \end{aligned} \quad (8.23)$$

And using Eqs. (8.6, 8.7),

$$n_{\pm} = 1 + 2\pi \sum_a N_a \{ \alpha_{(0)}^a + \chi_{(0)}^a \mp i\beta_{(0)}^a \pm i\gamma_{(0)}^a + [\pm i\alpha_{(1)}^a \pm i\chi_{(1)}^a + \beta_{(1)}^a] H_z \} \quad (8.24)$$

Here, β_0 is responsible for ellipticity (circular dichroism) and γ_0 is responsible for optical rotation. Thus, optical activity in the absence of external constant magnetic fields (native optical activity) is associated with β_0, γ_0 . These in turn, fix those parts of m and μ which are perpendicular to the fields of the electromagnetic wave. Now, $\alpha_{(1)} H_z \beta_{(0)}, \gamma_{(0)}$. Thus, native optical activity in the absence of external magnetic fields is of similar magnitude to that of magneto-optic activity. The above (Eq. 8.10) also indicates that magnetic optical activity exists as consequent to different polarizabilities from those of native optical activity. Also, note that MOR is consequent to $\alpha_{(1)}^a$.

Outside regions of absorption, then, and ignoring terms with, β, γ, χ [18]

$$n_{\pm} = 1 + \pi \sum_a N_a \{ \alpha_{xx}^a + \alpha_{yy}^a \} \pm i \{ \alpha_{xy}^a - \alpha_{yx}^a \} \quad (8.25)$$

$$\alpha_{\alpha\beta}^a = 2\hbar^{-1} \sum_j \{ 1/(\omega_{ja}^2 - \omega^2) \} [\omega_{ja} \text{Re} \{ \langle a | m_{\alpha} | j \rangle \langle j | m_{\beta} | a \rangle \} - i\omega \text{Im} \{ \langle a | m_{\alpha} | j \rangle \langle j | m_{\beta} | a \rangle \}] \quad (8.26)$$

Here, ω is the frequency of the incident radiation, $\hbar\omega_{ja} = W_j - W_a$ is the energy difference between the j^{th} and the a^{th} states. The electric polarizability is a consequence of the distortion of the occupied states, by the electric field of the other states, j .

Near regions of absorption, we have, [20]

$$\alpha_{\alpha\beta}^a = 2\hbar^{-1} \sum_a \overline{\chi}(\omega, \omega_{ja}) [\omega_{ja} \text{Re} \{ \langle a | m_{\alpha} | j \rangle \langle j | m_{\beta} | a \rangle \} - i\omega \text{Im} \{ \langle a | m_{\alpha} | j \rangle \langle j | m_{\beta} | a \rangle \}] \quad (8.27)$$

With $\overline{\chi}(\omega, \omega_{ja})$ a function to make the polarizability tensor finite at regions of absorption. Thus, the n_{\pm} are sums of terms which are in turn dependent upon the transitions between states, and their differing energy levels. The advantage of this approach is that we can observe the effect of adding terms regarding different electronic states to the overall refractive index.

It must be mentioned that plane polarized light can be seen as a superposition $m = +\frac{1}{2}$ to $m = -\frac{1}{2}$ of right and left circularly polarized wave states. Electrons in spin-down states may experience a transition to spin-up states by absorbing \hbar of angular momentum from a right-circularly polarized wave. Similarly, the interaction of a photon with left-circular polarization can cause a transition from the presence of a predominance of one type of electronic state will push the Verdet constant to a particular direction and magnitude. Also, the plane polarized wave, as a superposition of right and left circularly polarized states can produce bi-excitons, as two different electrons separated by \hbar in angular

momentum are simultaneously stimulated. Circularly polarized light, by contrast, can produce excitons, exclusively.

Other factors may contribute to energy level transitions of electrons, and thereby influence the size of the Verdet constant and its direction. The magnetic field, as is well known, produces Landau levels, with alterations of Faraday rotation, predicated upon transitions between the levels. Generally, and at room temperatures, the effects of Landau levels are washed out by thermal noise, $\hbar\omega_c \sim kT$, where ω_c is the cyclotron frequency and k is the Boltzmann's constant.

Also, the predicted and observed effects of Landau levels on Faraday rotation is the oscillation of optical rotation, as electrons in the bulk population are elevated above the Fermi level [21]. It is suggested here that such oscillatory effects may not be observed quantum dots with high levels of confinement, as these are truly structures of molecular dimension, and the number of electrons available for optical stimulation may be on the order of one to three. Thus, there would be no reserve population of electrons to elevate to the Fermi level, as in the bulk material.

In quantum dots, excitons and electrons experience confinement energies due to the effect of an infinite potential well. The coulombic energies of the excitons scale as $1/L$, where the confinement energies of the infinite potential well scale is $1/L^2$. At dot sizes of less than 10 nm [22], the confinement effects begin to predominate. Also, the exciton becomes uncorrelated, as the kinetic energy of the electron and hole due to the confinement. Ultimately, the Coulombic interaction of the exciton may, at sufficiently high confinement energies, be treated as a perturbation to the confinement energy.

Finally, the exchange interaction of the electron-hole is of greater importance with increased confinement, most particularly so, for strong confinement. This interaction mixes different electron and hole spin states, and is,

$$\hat{H}_{exch} = -\frac{2}{3} \epsilon_{exch} (a_0)^3 \delta(\mathbf{r}_e - \mathbf{r}_h) \sigma \mathbf{J} \quad (8.28)$$

where σ are the Pauli spin-1/2 matrices, \mathbf{J} are the hole spin 3/2 a_0 matrices, is the lattice constant, and ϵ_{exch} is the exchange strength constant [17,22]. Here, ϵ_{exch} can be calculated from,

$$\hbar\omega_{ST} = \frac{8}{3\pi} \left(\frac{a_0}{a_{ex}} \right)^3 \epsilon_{exch} \quad (8.29)$$

where a_{ex} is the bulk exciton radius.

Intermediate Range Order in Glasses: Boson Peaks and Nanoscale Inhomogeneities

The relations of the correlation volume to the distribution of relaxation times

The principal features of relaxation in the vicinity of the glass transition are nonlinearity (*i.e.* dependence of τ on structure) and nonexponentiality [39]. The latter property of structural relaxation kinetics require a relaxation function

$$\varphi(t) = \sum g_i \exp(-t/\tau_i)$$

involving a weighted distribution of relaxation times τ_i , where t is time and g_i are weighting coefficients [39, 40]. Equivalently, the kinetics may be described by an intrinsically nonexponential relaxation function, such as Kohlrausch-Williams-Watt (KWW) expression given by [39,40]:

$$\varphi(t) = \exp[-(t/\tau)^\beta] \quad (0 < \beta \leq 1).$$

$\langle \Delta^2 \ln \tau \rangle$ as given in equation (8.32) is a measure of the width of the spectrum or the distribution of relaxation times and can be directly related to the KWW β parameter for the above equation ($\beta \rightarrow 1$ as $\langle \Delta^2 \ln \tau \rangle \rightarrow 0$, $\beta \rightarrow 0$ as $\langle \Delta^2 \ln \tau \rangle \rightarrow \infty$) [41] Based on configurational entropy arguments and free volume concepts, Moynihan and Schroeder obtained expressions for $\langle \Delta^2 \ln \tau \rangle$ [41] In this work we rederive these equations starting with the more basic Adam-Gibbs premise.

Assuming that the mean relaxation time τ and the relaxation time τ_i of an arbitrary local rearranging region are given by Mohanty's and Adam-Gibbs' expressions [42-44]:

$$\ln \tau = -\ln A + z^* \Delta\mu / k_b T \quad (8.30)$$

$$\ln \tau_i = -\ln A + z_i^* \Delta\mu / k_b T \quad (8.31)$$

Here, A is the average rate for the state (E', V') to go to the state (E, V) at the same pressure (P) and temperature (T) where E (or E') and V (or V') are the total energy and the volume for the rearrangeable subsystem, respectively, $\Delta\mu$ is largely the potential energy hindering the cooperative rearrangement per molecule, z_i^* is the minimum number of molecules needed for a cooperative rearrangement in a local region, and z^* is the average value of z_i^* . At a given P and T it follows that

$$\langle \Delta^2 \ln \tau \rangle \equiv \langle (\ln \tau_i - \ln \tau)^2 \rangle = (\Delta\mu / k_b T)^2 \langle \Delta^2 z^* \rangle \quad (8.32)$$

where $\langle \Delta^2 z^* \rangle \equiv \langle (\ln z_i^* - \ln z^*)^2 \rangle$. We are interested here in the temperature dependence of $\ln \tau$ and $\langle \Delta^2 \ln \tau \rangle$ at constant P . Consequently $z^* = z^*(T)$.

At constant P and T the liquidlike fluctuations in an equilibrium melt are the fluctuations in the specific configurational entropy s_c and in the "free" or relaxational part of the specific volume v_f . At constant P in the equilibrium liquid:

$$s_c = s_c(T), \quad v_f = v_f(T).$$

Consequently, depending on whether we want to focus on the configurational entropy or on the free volume, we may write

$$z^* = z^*(s_c(T)) \quad (8.33a)$$

or

$$z^* = z^*(v_F(T)) \quad (8.33b)$$

It follows from Eq. (8.32) that at constant P :

$$\langle \Delta^2 \ln \tau \rangle = (\Delta\mu/k_B T)^2 (\partial z^*/\partial s_c)_p^2 \langle \Delta^2 s_c \rangle = (\Delta\mu/k_B T)^2 (\partial z^*/\partial T)_p^2 (\partial T/\partial s_c)_p^2 \langle \Delta^2 s_c \rangle \quad (8.34a)$$

or

$$\langle \Delta^2 \ln \tau \rangle = (\Delta\mu/k_B T)^2 (\partial z^*/\partial v_F)_p^2 \langle \Delta^2 v_F \rangle = (\Delta\mu/k_B T)^2 (\partial z^*/\partial T)_p^2 (\partial T/\partial v_F)_p^2 \langle \Delta^2 v_F \rangle \quad (8.34b)$$

The mean square fluctuation in the specific configurational entropy is [45, 46]

$$\langle \Delta^2 s_c \rangle = k_B v \Delta c_p / V_{AG}, \quad (8.35)$$

where v is the specific volume, Δc_p the difference between the equilibrium liquid and glass specific heats, and V_{AG} the correlation volume which are based on the Adam-Gibbs theory [41] $(\partial s_c/\partial T)_p$ is given by

$$(\partial s_c/\partial T)_p = \Delta c_p / T. \quad (8.36)$$

$\langle \Delta^2 v_F \rangle$ is given by the expression [41,46,47]

$$\langle \Delta^2 v_F \rangle = k_B T v^2 \Delta \kappa / V_{FV}, \quad (8.37)$$

where $\Delta \kappa$ is the relaxational part of the isothermal compressibility and V_{FV} the correlation volume which are based on the Cohen-Grest free volume theory [48]. $(\partial v_F/\partial T)_p$ is given by

$$(\partial v_F/\partial T)_p = v \Delta \alpha, \quad (8.38)$$

where $\Delta \alpha$ is the relaxational part of the thermal expansion coefficient. To obtain the $(\partial z^*/\partial T)_p$ term in Eq. (8.34) let us move directly to a Tool-Narayanaswamy equation interpretation [39, 40, 49] of Eq. (8.30). The equilibrium liquid temperature dependence of τ at a given temperature is given by:

$$(d \ln \tau / dT)_{eq} \equiv -(\Delta H^* / RT^2) = -(z^* \Delta\mu / k_B T^2) + (\Delta\mu / k_B T) (\partial z^* / \partial T)_p$$

while the glasslike temperature dependence of τ (for constant z^*) is given by:

$$(d \ln \tau / dT)_{z^*} \equiv -(x \Delta H^* / RT^2) = -(z^* \Delta\mu / k_B T^2).$$

Here ΔH^* is an Arrhenius activation energy and x ($0 \leq x \leq 1$) a non-linearity parameter which partitions the relative dependences of τ on temperature and structure. Taking the difference between these two equations we get

$$(\partial z^* / \partial T)_p = -(k_B T / \Delta\mu) [(1-x) \Delta H^* / RT^2]. \quad (8.39)$$

Inserting Eqs. (8.35) to (8.39) into Eq. (8.34) we finally obtain

$$\langle \Delta^2 \ln \tau \rangle = [(1-x) \Delta H^* / RT]^2 [k_B v / \Delta c_p V_{AG}] \quad (8.40a)$$

or

$$\langle \Delta^2 \ln \tau \rangle = [(1-x) \Delta H^* / RT^2]^2 [k_B T \Delta \kappa / (\Delta \alpha)^2 V_{FV}] \quad (8.40b)$$

The top expression on the right is of course identical to eq. (15) derived from the Adam-Gibbs theory by Moynihan and Schroeder [41]. The bottom expression on the right is identical to Eq. (20) derived from the free volume theory in their paper, except for the appearance of the $(1-x)$ factor in the present expression. The reason for this latter discrepancy is that Moynihan and Schroeder used the "classical" free volume expression in which the temperature dependence of $\ln \tau$ is contained entirely in the temperature dependence of $v_F^{-1} = (v - v_0)^{-1}$. In the present free volume treatment $\ln \tau$ depends explicitly on $1/T$ and in addition on z^* , which is in turn presumed to depend on v_F (cf. Eqs. (8.30) and (8.33)). The values of $V_{AG}^{1/3}$ and $V_{FV}^{1/3}$ from Eqs. (8.40a) and (8.40b) above are in much better agreement than was found for the corresponding values in the paper by Moynihan and Schroeder. From the Eqs. (8.40a) and (8.40b) we have

$$V_{FV}^{1/3} / V_{AG}^{1/3} = [\Delta c_p \Delta \kappa / T v (\Delta \alpha)^2]^{1/3} = \Pi^{1/3} \quad (8.41)$$

where Π is the Prigogine-Defay ratio [50, 51]: $\Pi = \Delta c_p \Delta \kappa / T v (\Delta \alpha)^2$. Since values of the Prigogine-Defay ratio Π near T_g are typically in the range 2 to 5, $V_{FV}^{1/3} / V_{AG}^{1/3}$ will lie in the range roughly 1.3 to 1.7. Intrinsic light scattering from liquids and glasses is due to density and concentration fluctuations [52,53]. Concentration fluctuations freeze at temperatures well above the glass transition temperature, T_g , so that time dependent scattering in the transition region is proportional to the time dependent mean square fluctuations, $\langle \Delta^2 \rho \rangle$ or $\langle \Delta^2 v \rangle$, in the density, ρ , or specific volume, v , due to local liquid-like structural variations [52,53]. Hence, the Rayleigh line intensity, I_R , or the Landau-Placzek ratio, R_{LP} , will be proportional to the distribution of relaxation times, $\langle \Delta^2 \ln \tau \rangle$.

Specific measurements of Rayleigh-Brillouin spectra as a function of temperature from glasses show a hysteresis curve in the scattering intensity in the vicinity of the glass transition region depending whether the measurement is done from low to high temperature or in the inverse sense. This observed hysteresis in the scattering and predicted from the above theory in the distribution of relaxation times is strong evidence for the formation of homogeneous regions representative of intermediate order in glasses. The magnetic behavior of the rare earth glasses should now be governed from particle like phenomena similar to the quantum dots.

The Boson Peak and the Density of Vibrational States and Intermediate Range Order (IRO)

Raman scattering in disordered systems differs from the scattering in crystals in that it is related to spectrum of the vibrations in the material. Experimentally Shuker and Gammon [54,55] showed that the entire Raman spectra of glass consisted of broadened intensity lines (not the sharp spectral lines, as seen in crystals). The crystal state follows precise selection rules due to \mathbf{k} -conservation resulting in relatively narrow Raman lines. In the glass counterpart the selection rules are broken because the disorder in a glass allows momentum conservation to be of no consequence and the Raman lines are extremely broad. This is also valid for the low frequency "Boson peak" - but remember its crystal counterpart does not exist. According to Shuker and Gammon [54,55], the intensity as a function of frequency for Raman scattering is given by equation (8.41) in the previous section and we will rewrite this equation again. It was shown that the intensity of the Raman spectra in disordered solids is

proportional to the density of vibrational states $g(\omega)$ multiplied by light vibration coupling coefficient (Pockels' coefficient) $C(\omega)$:

$$I(\omega) = g(\omega) C(\omega) [1+n(\omega)] / \omega ; \quad (8.42)$$

here $[1+n(\omega)]$ is the Bose-Einstein occupation number for the Stokes component. So it is possible to find $g(\omega)$ from Raman spectra, if one knows the frequency dependence of $C(\omega)$. In the first discussion [54,55] it was supposed that $C(\omega) = \text{constant}$, but this dependence does not lead to the correct $g(\omega)$. In the extreme case of complete randomness of the atomic couplings or the atomic amplitudes in the vibrational modes $C(\omega)$ would be independent of frequency.[56]. Comparison of the Raman spectra with inelastic neutron scattering data (which yield in the incoherent approximation directly $g(\omega)$) have shown [57-60] that in the the Boson peak region, $g(\omega)$ exhibits a broad maximum in a number of glasses, while $C(\omega)$ has no maximum and varies nearly linearly. As discussed by numerous other authors [61-67] the Boson peak is due to an increase of the vibrational density (phonon density) of states over the Debye value ($g(\omega) = 3\omega^2 / \omega_D^3$, $\omega_D = \text{Debye cutoff frequency}$), and this origin is now generally accepted.

The Boson peak is caused from vibrational excitations made up of acoustic phonons most likely shear or transverse phonons which scatter strongly from elastic inhomogeneities in the structure due to the topological disorder in glasses. The scattering leads to a drastic decrease of the mean free path of vibrations $L(\omega)$, and, in particular, can increase the vibrational density of states in a certain frequency range. These excess phonon states may now be considered to be localized by the strong scattering. Hence, phonon localization may be viewed in terms of the Ioffe-Regel rule [68,69]. The Ioffe-Regel criteria are given as:

$$k(\omega_{\text{IR}}) L(\omega_{\text{IR}}) \approx 1, \quad (8.43)$$

with $k(\omega_{\text{IR}})$ -the magnitude of wave vector, $L(\omega_{\text{IR}})$ -the mean free phonon path at the Ioffe-Regel frequency ω_{IR} . (Note: The phonon localization here is analogous to the Anderson localization of electrons.) The Ioffe-Regel rule allows us to calculate a correlation length in terms of ω_{BP} , the Boson peak frequency, and the sound velocity, v_s . Expressing this rule thusly,

$$L_c \approx v_s / \omega_{\text{BP}} \quad (8.44)$$

The excess density of phonon states can be attributed to the consequence of strong scattering [70]. Now, the position of the Boson peak maximum leads to correlation length that is an indication of the intermediate range order (IRO) in glasses. These correlation lengths or IRO's will be on the order of several nanometers in size.

Note that the intermediate range order has also been interpreted as a nano-scale inhomogeneity with respect to the anomalous Rayleigh scattering (hysteresis effect in the Landau-Placzek ratio) and here we have postulated that the region is homogeneous (domains) up to nanometer size extent. A clear difference is shown from the accepted short range order concept, which has governed the behavior of amorphous solids for so long. The observations done in this work, that a typical correlation length or IRO for a glass extends over several nanometers in length certainly gives new insights to understand basic properties of glasses.

Summary Comments on Boson Peaks and Nanoscale Inhomogeneities

Both of the above sections (8.30, 8.31) predict results for glasses which may have drastic implications with respect to the observed behavior for Faraday rotation in the rare earth containing glasses. The quantum dots of the II-VI semiconductors in the glass matrix exhibit a nonlinear behavior with the formation of kinks at certain values of the applied field which seems to be particle size dependent. The rare earth containing glasses show a similar result from their Faraday rotation behavior and with external field values lower than the quantum dots. It may very well also be a particle size dependent phenomenon. Which asks the question why is there particle like structure in a glass similar to the quantum dot structure responsible for its magnetic properties? The intermediate range order as obtained from the Boson peak measurement for glasses by Raman scattering or the Nanoscale inhomogeneities obtained from Rayleigh-Brillouin scattering results, with both measurements complementing each other allow us to draw a conclusion that particle like regions exist in the glass, with these regions have typical diameters also on the order of the quantum dot diameters. The rare earth oxides which persist interstitially in the glass matrix may well be confined to these regions of nanoscale inhomogeneities and the particle like behavior is explained by such a mechanism.

Light scattering from glasses in the glass transition region exhibits an anomalous Rayleigh scattering. We observe a maximum in the scattering intensity versus temperature during heating. This behavior is consistent with the presence of nanometer-scale inhomogeneities (density fluctuations) which relax at differing rates. In all cases, a hysteresis effect is seen in the light scattering data taken during heating and cooling each sample from room temperature through the glass transition region. We suggest that this could be the source of non-exponential structural relaxation kinetics. Here we do the necessary calculations to show the relations of the correlation volume to the distribution of the relaxation times. From these approaches, we calculate the correlation volume of these nanoscale inhomogeneities and find a typical size ($\sim V^{1/3}$) of about 2-3nm. This is consistent with independent observations done by Raman scattering where we observed the low energy "Boson Peak". For the low frequency Raman spectra, all glasses show a broad feature around 0.6-3.0 THz, the so-called Boson peak. This Boson peak is associated with the existence of intermediate range order in the glass. The Boson peak is due to an increase in the vibrational density of states, over the Debye value, caused by localized excitations (phonon localization). The degree and range of disorder in the glasses is obtained in a quantitative sense from the behavior of the Boson peaks with temperature and compared to Rayleigh-Brillouin scattering data for the same glasses.

Hence, we wish to imply that the complementary concepts of Boson peaks from Raman scattering and the nanoscale inhomogeneities from Rayleigh scattering lead to the same concepts of intermediate range order in glasses. This intermediate range order manifests itself in a homogeneous region of a typical extend from 2-4 nm in size surrounded by a disordered extended surface. This concept applied to the rare earth containing glass samples allows one to postulate that the rare earth oxides are enclosed in this homogeneous region and their magnetic behavior should now be governed by a particle like process similar to the quantum dot samples.

Experimental Techniques

The quantum dot samples were prepared, using Schott-RG695 glass, which was bleached (struck) first, at 1100°C and cooled to room temperature. The "striking" removes any nano-crystallites from the glass. Then these glasses are heat treated for varying lengths of time to obtain different sizes for the quantum dots. With sufficient time larger diameter dots grow at the expense of smaller dots. This

occurs as smaller dots dissolve back into the glass matrix and larger dots grow at their expense. This base glass was a borosilicate glass with the primary constituents being SiO_2 , B_2O_3 and minor constituents of Na_2O , CaO , K_2O and ZnO , all in the approximate ratios of 75:13.6:6.4:4.5:0.4, respectively. This base glass was doped with Cd and S, Se. Samples heat treated for longer periods of time had a higher degree of homogeneity than did the samples treated at higher temperatures for shorter periods of time, as determined from their absorption spectra peaks. More homogeneous CdSe samples were of greater sphericity, and varied in size approximately 7%, as opposed to a 30% for the less homogeneous samples [35]. Sizes were measured by a technique involving low frequency Raman scattering and the analysis of the absorption spectra for various samples [36].

Figure 2 shows the data used to calculate the average diameters of the CdSe quantum dots.

A variety of samples were studied, in which glasses containing rare earth oxides were evaluated for Faraday rotation as a function of an applied external magnetic field. These samples contained 33% rare-earth oxides in a sodium silicate base glass. These samples were prepared employing standard small batch glass forming techniques. Optically these glasses all exhibited low Rayleigh scattering as determined from Landau-Placzek ratio measurements [J. Schroeder-unpublished data].

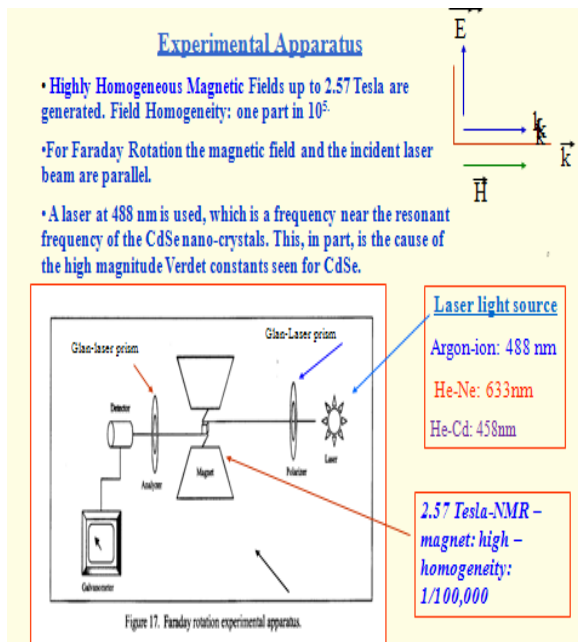


FIGURE 8.1

A schematic of the experimental apparatus employed in the Faraday rotation studies

For the Magneto-optic studies the samples were placed in the gap of a “Magnion” electromagnet (NMR magnet with high field homogeneity, 1 part in 10^5) with field self-regulation and a maximum field up to 2.57 Tesla. A schematic of the experimental apparatus is given in Figure 1. Note the Faraday geometry, the polarized light propagating vector and the magnetic field direction being parallel or antiparallel, is employed in the measurements. The light source consisted of either a helium-neon laser, at 633nm (50 mw) or mostly an Argon-ion laser at 488nm (500 mw) passed through the long axis of the samples (Faraday geometry) with the aid of a pair of mirrors placed at 45° from the angle of the incident beam to allow for the laser to be parallel with the applied magnetic field. The laser beam was collimated

with two pinholes of the same diameter to assure that the light beam was always contained within the thinnest sample. The entire system was calibrated by using a standard sample of Corning 8463 glass and SiO₂ glass (homosil). A glan-laser prism was placed before and after the sample as polarizer and analyzer, respectively. The beam intensity was read with a photo-detector and electrometer. The analyzer was set to 45° from the null point.

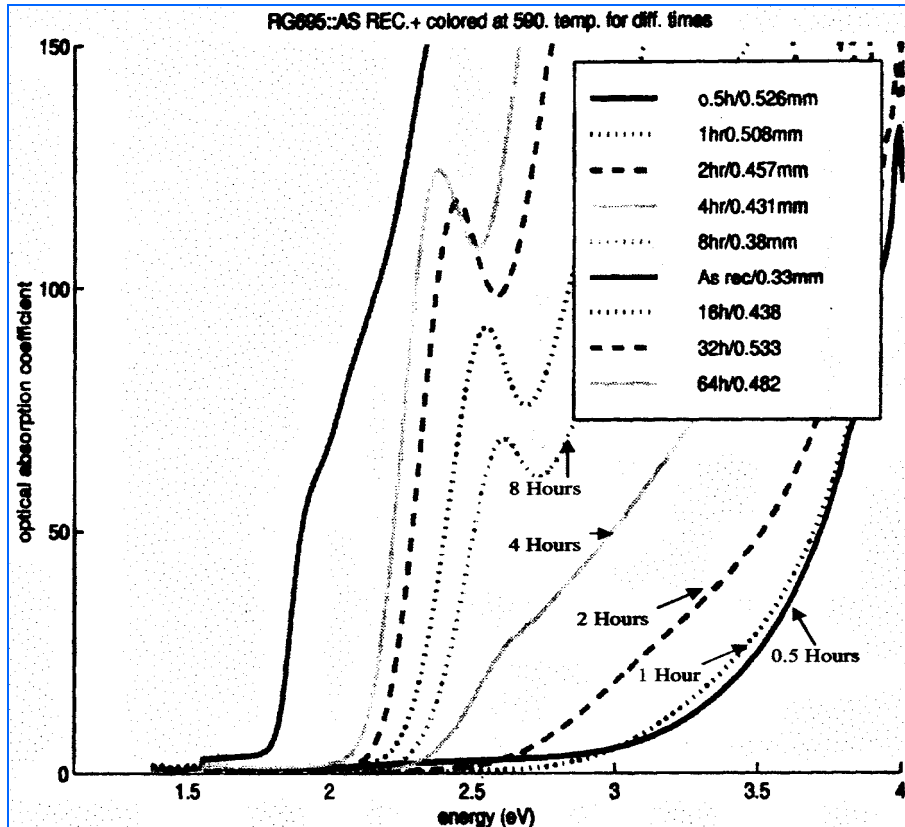


FIGURE 8.2

A typical data run of Optical Absorption Data versus excitation energy for various quantum dot composites. Here we show spectra for CdSe quantum dots. The method is shown by which the particle size of the quantum dots were determined. It also shows a red shift in wavelength as the particle size of the quantum dots become larger or the samples treated for 1, 2, 4, and 8 hours have progressively smaller energies at the absorption peaks

Figure 3 shows a Faraday rotation measurement versus applied magnetic field for the base glass for the oxide containing glasses. It is clearly seen that only one slope exists up to the highest external field value for this Sodium-Silicate glass sample.

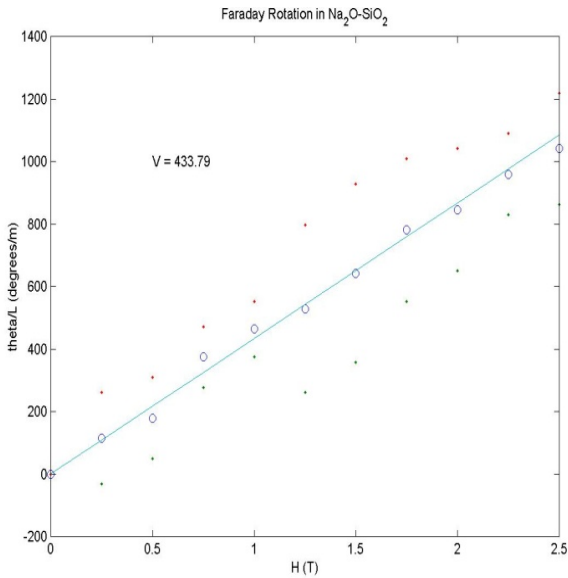


FIGURE 8.3 Faraday rotation measurements for the standard sodium-silicate glass to which the rare earth oxides were later added. Note the single slope and no evidence of any “kink” development is seen throughout the external magnetic field range

Results

A set of Faraday rotation measurements were done on samples consisting of CdS and CdSe quantum dots contained in a borosilicate-glass matrix.

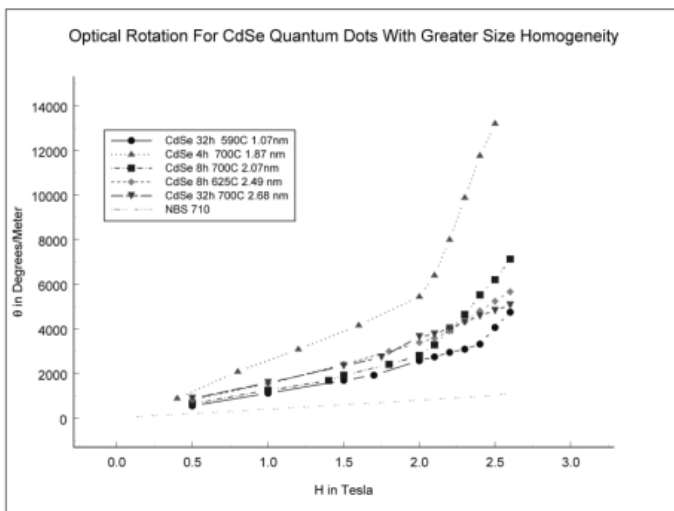


FIGURE 8.4 Optical Rotation of CdSe quantum dots with less homogeneity and greater size dispersion (~30%). (Estimated error from averaging a number of data runs is ± 50 degrees/Tesla-Meter)

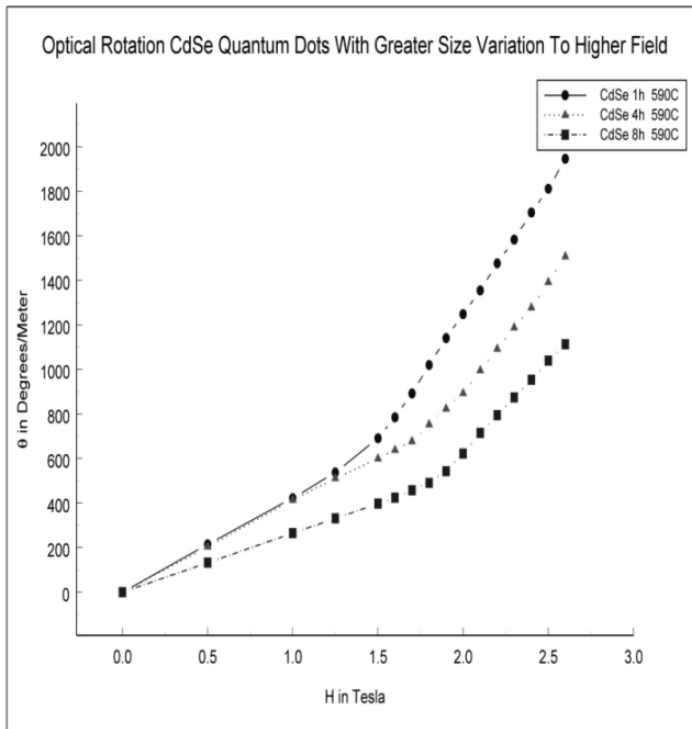
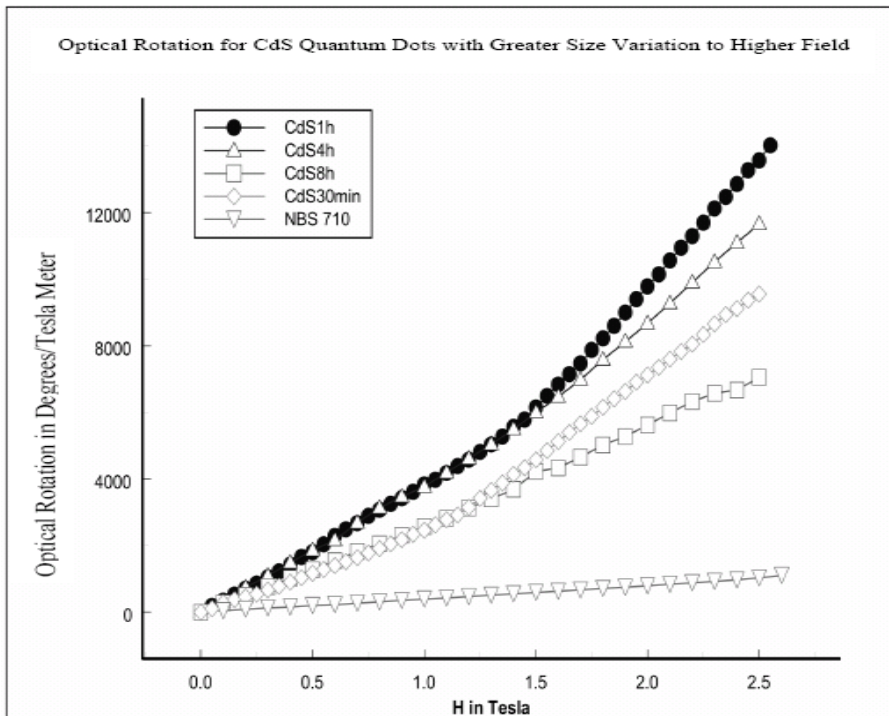


FIGURE 8.5

Faraday rotation for CdSe quantum dots in a glass matrix with greater particle size homogeneity (only ~ % variations). This size dispersion has an effect on the magnitude of the slope of the Faraday rotation with respect to the magnetic field

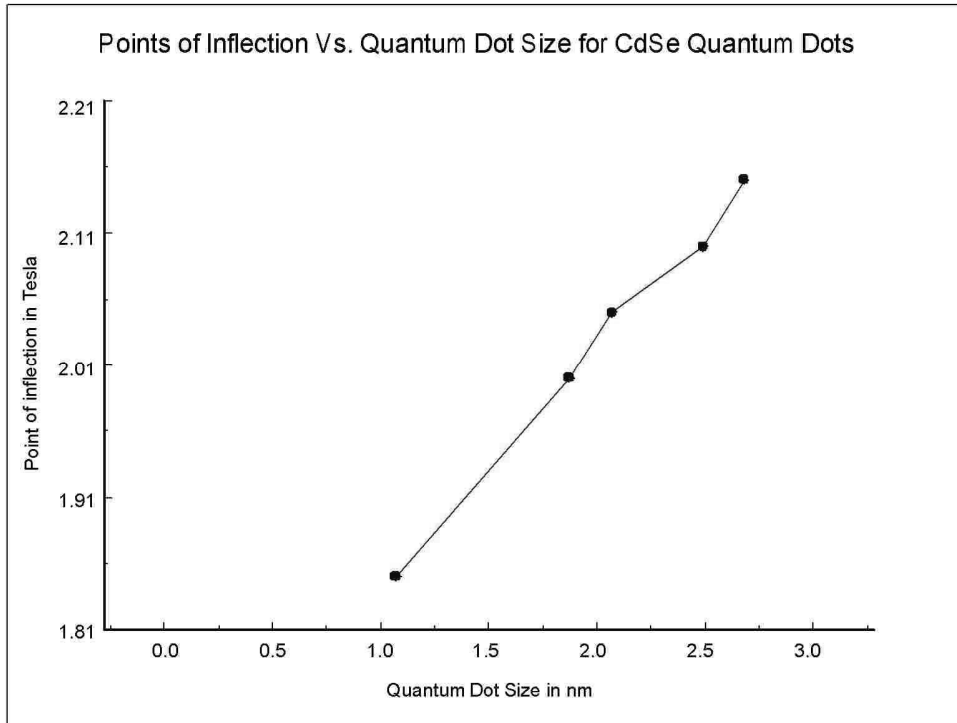
See Figures 4, 5 and 6 where a striking effect is obvious that the Faraday optical rotation is not linear as a function of the applied field for all three figures. The onset of this inflection or “kink” in every case occurs at different applied field values and the sample with the smallest quantum dot size has this inflection at the lowest value of the external applied magnetic field. Note in the figures that the samples with the shortest heat treatment times will be those of the smallest quantum dot diameter.

**FIGURE 8.6**

Optical rotation of CdS quantum dots in glass for high homogeneity samples. Error bars the same magnitude as in figures 4 and 5. Measurements for a NBS-710 glass is also shown as the lowest line in the graph

In Figure 6, measurements of Faraday rotation versus applied field are also shown for a NBS-710 glass sample and the “kink” is absent in this glass up to the highest field value attained and its Verdet constant is considerably lower than any of the CdS or CdSe containing glasses. Another effect to be noted upon comparing the results from Figure 4 and 5, both are CdSe quantum dots, but CdSe containing samples in Figure 4 have a greater size variation ($\sim 30\%$) compared to CdSe samples in Figure 5 which are of greater homogeneity ($\sim 7\%$) and have greater sphericity. The interesting effect here also shows that homogeneity of the particle size and sphericity (steric effects) affect the magnitude of the Faraday rotation. Comparing the magnitude of the Faraday rotation, for the smallest quantum dot size of the samples given in Figure 4 and Figure 5, there is about a seven-fold increase for the smallest quantum dot diameter with the higher homogeneity sample having the greater Faraday rotation. The samples heat treated for times longer than eight hours demonstrated little if any “kinks”. Hence, optical rotation of homogeneous CdSe QDs demonstrates increased Verdet constants with increasing confinement (decreased dot size).

Also where inflection points are seen for the samples, there is a linear relationship between the QD radius and the field H at which each “kink” occurs and Figure 7 demonstrates this for the CdSe sample.

**FIGURE 8.7**

Field intensity at the point of inflection versus quantum dot size for CdSe samples

That the quantum dot size versus points of field inflection maintains a linear relationship may at first point to a relationship between the observed “kinks” and the extreme confinement energies. However the electronic levels in QD’s increase with an inverse quadratic behavior with dot size, which itself is related to the confinement energies; therefore one would expect there to be a quadratic and not a linear relationship between the external applied magnetic field at the transition and the dot size if the kinks were simply dependent upon the confinement energies.

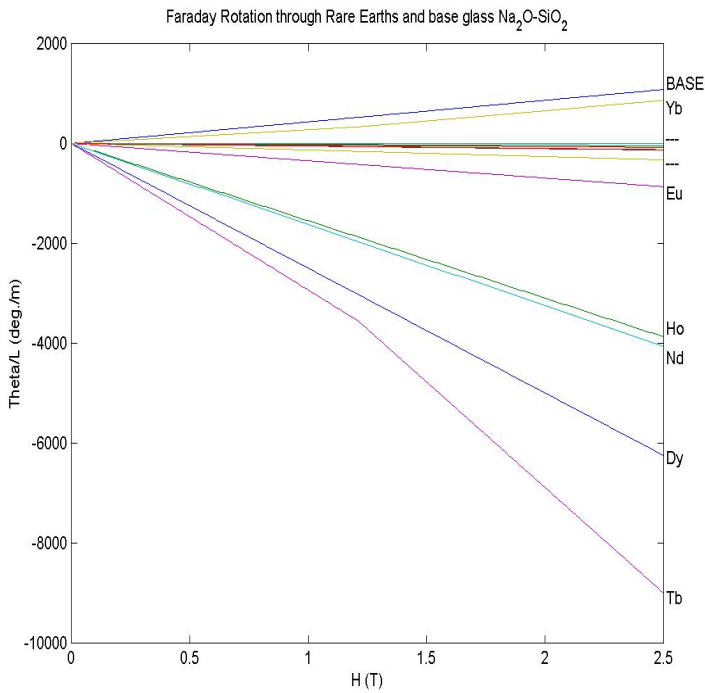


FIGURE 8.8

This plot shows all the rare earth containing samples used in this experiment. The value for the slope of each line is the Verdet Constant for that sample. Positive slopes are diamagnetic and negative slopes are paramagnetic. Note the larger Faraday rotators: containing TbO, DyO, NdO, HoO

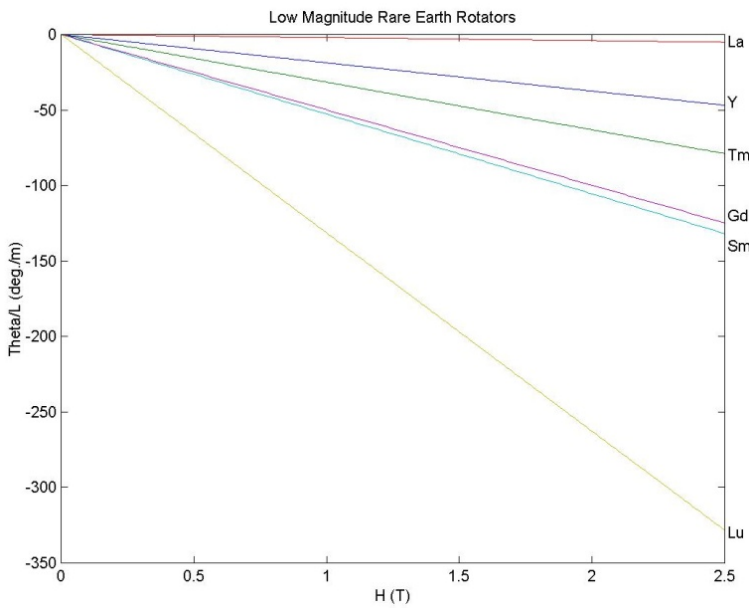


FIGURE 8.9

Low magnitude rare earth rotators-no kinks observed

Figures 8 and 9 show a compilation the results of Faraday rotation measurements for all of the rare-earth containing glasses. Terbium-oxide, Dysprosium oxide and Holmium oxide containing glasses demonstrate points of inflection (kinks) at higher value of the applied field. This certainly is an unexpected result. Note that these particular rare-earth containing samples (Tb, Dy and Ho) with “kinks” had the highest Verdet constants in the linear range. Enlarged versions with the data points for rare earth containing glasses with TbO, YbO and HoO rare earth oxides are shown in Figures 10, 11, and 12 ; respectively.

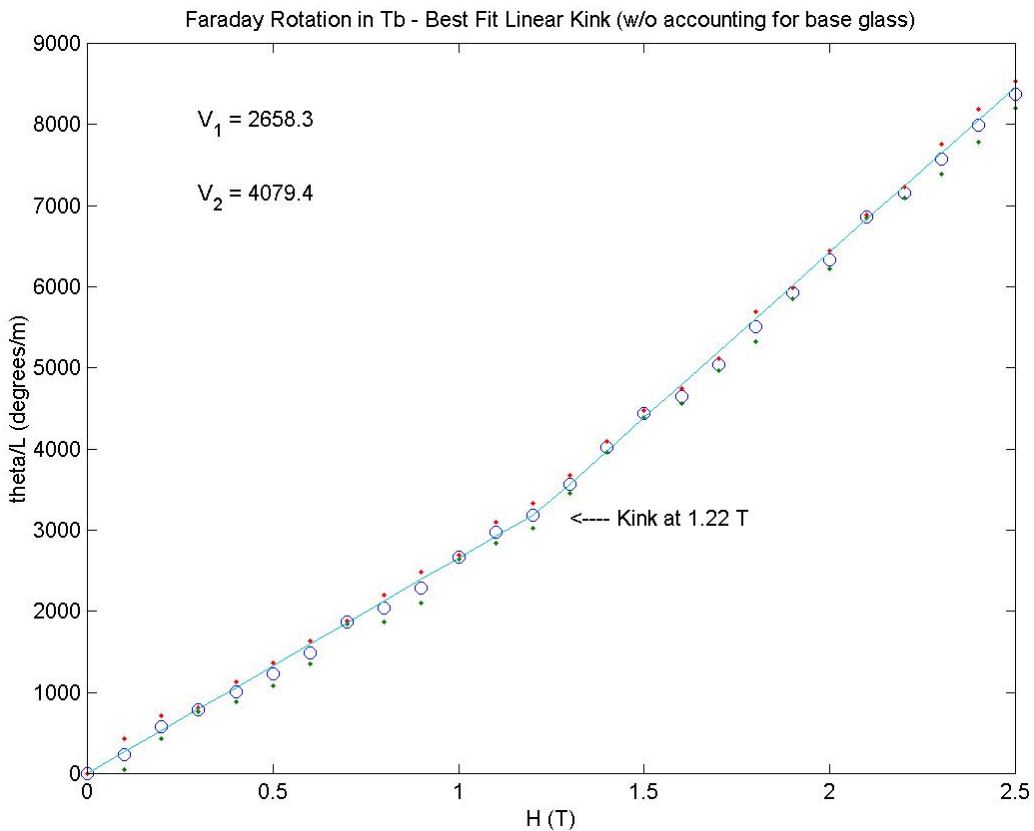


FIGURE 8.10

A Typical Data Run of the Terbium-oxide-containing glass sample. A visible kink or inflection point is present at ~ 1.21 T. V_1 and V_2 are the changes of the Verdet constants

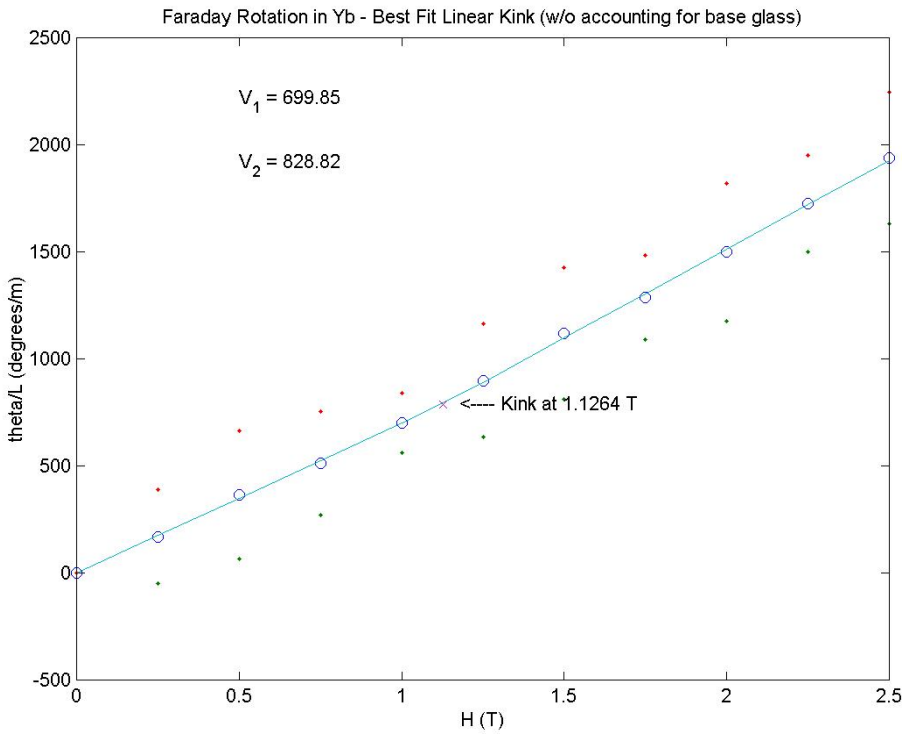


FIGURE 8.11
 YbO-containing glass Faraday rotator. An inflection point is seen at 1.126 Tesla

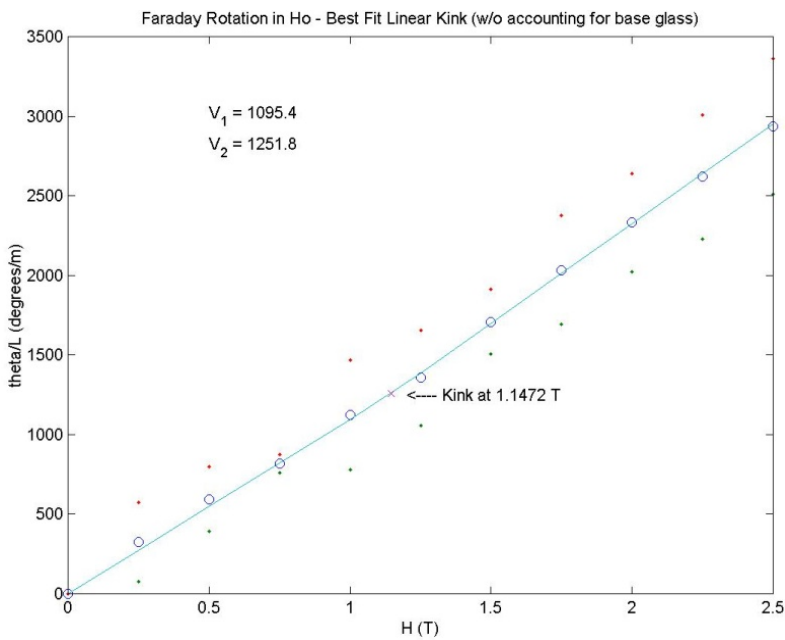


FIGURE 8.12
 HoO containing glass-Faraday rotation versus external magnetic field. Inflection point is clearly evident

A single crystal sample of NaCl was also examined and no evidence for an inflection point was seen. This result is given at the bottom of Figure 13.

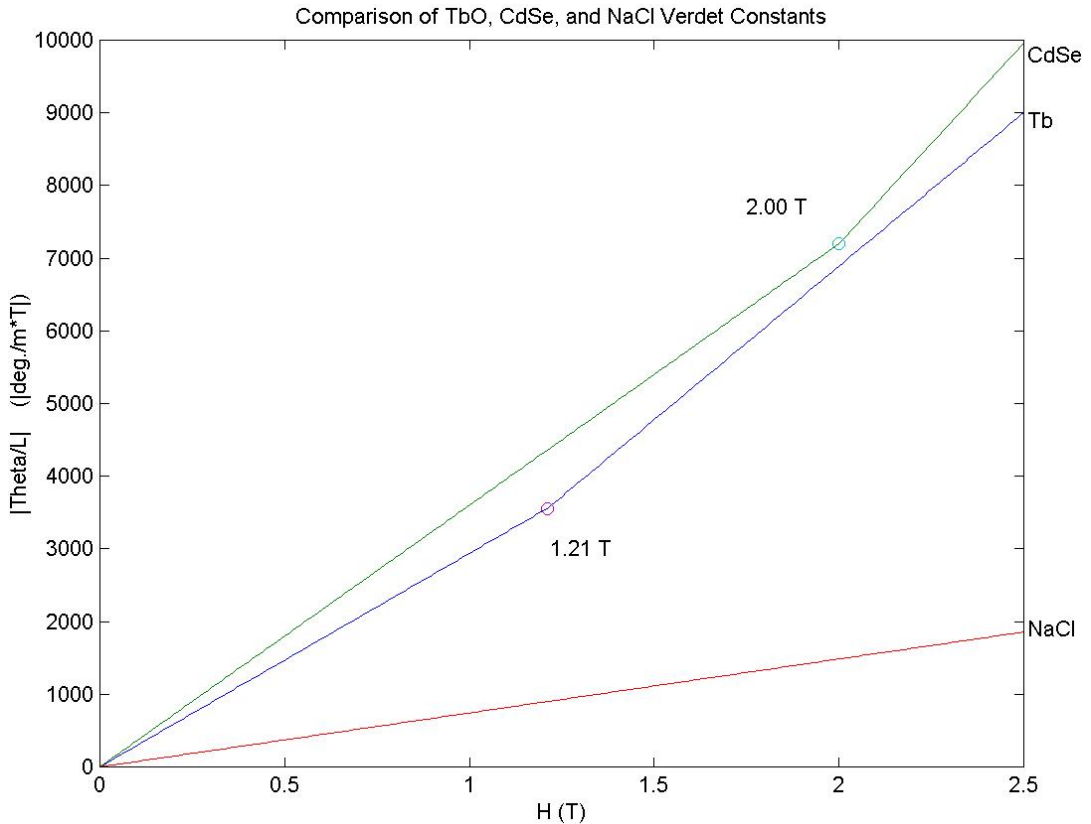


FIGURE 8.13

This figure compares the Verdet Constant of a CdSe nanocrystal glass with the results of multiple runs of the TbO doped glass and the single crystal NaCl sample. It is clear that the TbO sample displays an instantaneous increase in Verdet constant after a certain magnetic field intensity value just like the quantum dots of CdSe. This may suggest 3-D electron confinement and intermediate range order domains in the silicate base glass. Note there is no slope change in Verdet Constant for the single crystal NaCl

This figure also shows a comparison of CdSe quantum dots, TbO glass and single crystal NaCl, with respect to the Faraday rotation measurements. Figure 8 shows a compilation of the rare-earth containing samples and their base glass of $\text{Na}_2\text{O}\cdot\text{SiO}_2$, and note that most of the glasses are paramagnetic with the base glass and Yb being diamagnetic. Figure 9 exhibits the remaining low magnitude rare earth rotators.

In the following section the observed effects will be discussed and possible mechanisms will be proposed to try to explain the observed results, especially the inflection points (kinks) in quantum dot containing glasses and some of the rare-earth glasses.

Discussions

Various mechanisms are to be put forth, evaluated and discussed as to the feasibility of using these processes to explain the observed effects as given in the results. Let us consider Landau levels, resonance effects, shape (steric) and piezo-electric effects, electron-spin correlation and the intermediate range order of the glass matrix itself and try to interpret how each of these mechanisms may or may not affect the Faraday rotation behavior.

The size of the Verdet constants seen for the samples used in this study is significantly larger than a typical standard glass SiO_2 and significantly greater than for the base glass. It is significantly higher for the more homogeneous CdSe samples than for those samples less homogeneous in size distribution. Additionally, the more homogeneous samples were grown at lower temperatures (close to the glass transition temperature) for longer periods; not only allowing greater size homogeneity but also greater sphericity. The presence of less than spherical edges causes charge build-up at the vertices of the crystal. This, in turn, alters physical parameters such as exciton correlation [71]. The lack of sphericity in quantum dots may cause the electron and hole to occupy different positions in the quantum dot, thus making exciton formation difficult. Such charge polarization would undoubtedly alter electron and hole motion in general and could clearly alter the electronic properties of the quantum dots in question. The magnitude of the Faraday rotation of homogeneous versus inhomogeneous CdSe quantum dots in a glass matrix is greater by a factor of almost 7 as seen from Fig.4 and 5. The increased sphericity of the more homogeneous dots may be a factor in this increase.

Landau levels are a consequence of an externally applied magnetic field to a material with free electrons.[38] The application of an harmonic oscillator model will characterize their energies and electronic motion. The energies of Landau levels are $(n + \frac{1}{2}) e\hbar\omega_c/2\pi c$ with e , \hbar , c , H being the elementary charge of the electron, Planck's constant, the speed of light and the magnetic field, respectively.[72] For an unconfined electron in a Landau level, the ground state energy is ~ 1.7 meV. Thus, the measurement of phenomena involving Landau levels generally involves very low temperature processes. Let us consider Landau levels and magnetic flux. The electron's wave function surrounds a closed path and the magnetic flux enclosed within such a path is quantized in integer multiples of the flux quantum, $\Phi_0 = hc/e$. The degeneracy, g , is the total magnetic flux measured in units of the flux quantum, $g = \Phi / \Phi_0$. The total degeneracy for a two-dimensional Landau level in a three-dimensional quantum dot is $g = \pi r^2 (\Phi / \Phi_0)$. However, the magnetic flux quantum is $\approx 2.10^{-15}$ Wb. For a 1T field, the expected magnetic flux within a 1 nm quantum dot $\approx 3.10^{-18}$ Wb. Classically, the external magnetic field would have to be ~ 100 T to reach a degeneracy of one and the first Landau level.

Our measurements were made at room temperature, with $kT \approx 28.5$ meV. Classically, the first Landau level has energy of 1.7 meV, well below the thermal threshold. Using a semiclassical approach and setting $m\omega^2 r^2/2 = \hbar\omega(n + \frac{1}{2})$, for $n = 0$, we obtain $r \approx 25$ nm. From the WKB approximation [73,74] the energies of a confined harmonic oscillator with a confinement ratio of 0.5 the classic harmonic oscillator potential increases the ground state energy by a factor of ~ 4 or it behaves approximately as $1/r^2$. By extrapolation a confinement of 0.10, the size of the largest quantum dots studied would give a ground state energy increased by a factor of ~ 100 , resulting in a ground state Landau level energy of ~ 170 meV, well above the thermal background. Given the calculated high magnetic field intensities (≤ 300 T) necessary for Landau levels to exist in small quantum dots, it is considered unlikely that they play a role in the interactions seen [75]. Hence, it is likely that the issue of Landau levels being associated with the kinks in the Faraday rotation curves will have to be set aside.

In the discussion let us next consider resonance effects. See preliminary concepts in the theoretical background section above. The magnitude of the Verdet constants of the quantum dot containing

glasses is significantly greater than its base glass or the standard SiO_2 glass. The Verdet constants are also significantly higher for more homogeneous samples than those samples less in size distribution. For CdSe quantum dots it is greater by about a factor of seven. Considering that the smallest of the more homogeneous CdSe quantum dots have band gap energy of 2.54 eV. Whereas the exciting light of the argon-ion laser (488 nm) has energy of 2.56 eV. Thus the energy of the exciting light is essentially on the band edge for this quantum dot. It is well known that the Verdet constant equations predict resonance effects as seen from the theory background section.

In the samples of quantum dot containing glasses with size heterogeneity of significant variation, the polarization vectors for light exiting the different quantum dots may exist not as a plane polarized beam but as an ensemble of waves with the phase relationship no longer unique. This in fact may lead to nonlinear effects as predicted by the theory of Yu and Osborn [36]. Thus the optical rotation would be significantly less for samples with large heterogeneity than very homogeneous dot distribution in samples. In the later case the majority of the exiting waves had essentially the polarization or the same phase relationship. This may explain the difference in the Faraday rotation as seen in Figures 4 and 5 [75].

The energy of the incident laser is approximately 0.02 eV from the edge of the bandgap of the smallest quantum dot. This fact, based on the resonance effect would account for the higher Verdet constants of the quantum dot containing glasses. It does not, however, explain the kinks since the edge of the band gaps of the larger quantum dots deviate by more than 0.5 eV from the energy of the incident laser light.

Next let us consider shape (steric) and piezoelectric effects on the Faraday rotation. Heat treatment at temperatures nearer to the glass transition temperature for longer periods of times tends to produce more spherical quantum dots with higher homogeneity of size. Computer modeling of quantum dots has demonstrated significant charge build-up at sharp vertices of quantum dots [71]. More spherical dots have much less charge build up. This charge build-up tends to isolate electrons and holes, causing them to become uncorrelated. It also causes confinement of electrons to the central position of the quantum dot. This in turn alters physical parameters such as the exciton correlation [71].

Kinks in the Faraday rotation from rare-earth containing glass samples have also been measured. These kinks have an on-set magnetic field value that is lower than for the quantum dot case. This raises the possibility of potential bounded regions of intermediate range order of 2-10 nm in size, and such regions are established from Raman measurements of Boson peaks [38, 75]. These regions or domains present a unifying factor between kinks in the quantum dots and the kinks seen in the rare-earth doped glasses. These potential bounded regions in the glasses may serve as regions of electron and phonon confinement [76], bringing into play similar physical factors. It is these physical factors which may be responsible for the kinks seen in both materials. It may be that quantum dots in colloidal form will not show nonlinearities, and only the intermediate range order (IRO) of the glass makes the kinks a possibility. When Faraday rotation measurements were done on a single crystal NaCl sample, no kinks were detected. Its Verdet constant was linear throughout the magnetic field range.

The presence of electron-spin correlation may be involved in the kinks seen in the Faraday rotation curves in both sets of materials. Quantum dots present potential bounded regions, and rare-earth containing glasses may as well. Electrons confined in these regions may evidence correlations of their spins which would be expected to affect Faraday rotation. As given by Holstein and Primakoff [77,78] regions of spin correlation would substantially increase the energy of interaction between electron spins, thus tending to keep the electron in a spin aligned state. Spin exchange is a process in which the energies of two electrons are lowered by a quantum mechanical interaction, in which their spins are "exchanged", or in a sense linked. The energy for spin exchange in a ferromagnetic material are ~ 160 meV per electron pair. We may link at the electrons in quantum dots, elevated from the valence to the

conduction bands, as being free electrons. The treatment of spin exchange interactions for such free electrons is a special case and the interaction energy takes the form $E_x/N = -\frac{3}{4} e^2 (3\rho/\pi)^{1/3}$. The derivation of this equation will be treated later in this section. Now if the density of electrons is taken as the density in a quantum dot of radius 1 nm, and if we multiply the right side of the above equation by $1/\epsilon$, the dielectric constant for CdS, CdSe it is approximately 9.35-10.2, we obtain for a three electron quantum dot, ~ 200 meV per electron. This energy compares favorably with the ferromagnetic spin exchange energy. Thus the factor ρ will be lower for larger quantum dots and the exchange energy per electron will therefore be lower. If this is the case, then it is further possible that a larger externally applied magnetic field would be necessary to provide the impetus to align the spins in larger quantum dots; thus causing the linear relationship between quantum dot size and the magnetic field intensity at which the kinks are seen, as is noted experimentally.

We are therefore presented with a phenomenon in which kinks in the Faraday rotation curve are noted for semiconductor nano-crystals in glass matrices, as well as for some rare earth containing glasses. The base glass does not demonstrate kinks in its Faraday rotation curve, nor does the NaCl crystal. This therefore begs the question as to what possible similarities might exist between samples of semiconductor quantum dots embedded in glass matrices and rare earth-containing glasses. A possible explanation is the structure of the glasses themselves. Glasses exist on a continuum between the crystalline and the liquid or gaseous state. Here, [38,41,75,76], it is noted that glasses represent a physical state in which, in effect, a glassy liquid is cooled very rapidly (quenched) than it may for a crystal. The net result is that it becomes an amorphous solid, with regions of nanoscale inhomogeneities; which then has some characteristics of crystalline materials. The glass structure has bonds, similar to the crystal. The spatial symmetry of the crystal is lost, however, and the periodicity is compromised as well, as a consequence, however, correlation between atoms exists. For gaseous materials, there is no correlation between the atoms. Liquids occupy a position between glasses and gases. Atoms/molecules are in physical contact, but they are not rigidly bound to each other, and there is no clear long-term order or correlation. There is, however, physical contact and collisional motion.

Experimental evidence exists which supports the contention that there exists intermediate-range order in glasses [38,41,75,76,58,80-82,83]. There is evidence stemming from Raman spectroscopy in which low-lying Raman vibrational peaks termed "Boson peaks", are associated with what has been termed, "intermediate range order" [38,41,75,76] in glasses. The intermediate range order, of the order of 2–6 nm appears to be independent of glass composition, and is thus a robust phenomenon. More specifically, the intermediate range order may be thought of as a phenomenon in which electrons and phonons are localized within glass matrices by the amorphous nature of the glass itself (intermediate-range order, manifesting itself in 2–6 nm. domains). The glass matrix does have order and there may be areas of structure similar to that of a crystal, surrounded by regions which are much less ordered. It is these surrounding areas of disorder which may provide a potential barrier, effectively confining electrons and phonons into regions. As stated in Reference [64], the wavefunction effectively occupies an area near a center of several atoms. Away from this area, the probability amplitude decays exponentially. This decay goes as $\exp(-\alpha r)$, the term, α being the "inverse localization length". The "confinement" of the electrons and phonons in these regions effectively occurs as a consequence of a "disorder induced potential energy of sufficient strength" [82]. And, in contrast to the quantum dot, where there is assumed to be a fairly consistent potential barrier at the order of the nanocrystallite, there is a more inhomogeneous potential barrier in the confined regions in glasses. There is a distribution of barrier heights, denoted by an averaging parameter, W , giving the width of the distribution. Thus, we may postulate the existence of localized regions of order in glasses (nanoscale inhomogeneities), surrounded by disordered regions, effectively producing regions acting as de facto

quantum dots. These regions would function as quantum dots, in that there would be localization of electrons and phonons in regions surrounded by a potential barrier of sufficient magnitude to produce localization. From a theoretical standpoint, these regions would likely be difficult to model, as by their very definition, they would be amorphous. They would also be non-spherical, and as such, would be subject to significant piezoelectric effects, with the attendant separation of electrons and holes this produces. In the glasses doped with rare earth ions, they would also contain ions with multiple unpaired f-orbital electrons. Thus, we may view these glasses as containing de facto quantum dots with rare earth ions. Henceforth, these regions will be termed “potential-bounded regions” (PBRs) for brevity and to prevent confusion. Viewed as such, it is interesting that these glasses have Faraday rotation curves which have kinks at field intensities significantly lower than for the semiconductor quantum dot samples. Note that for the smallest of the homogeneous CdSe quantum dot samples the first inflection was at 1.85T, whereas for the glasses containing TbO it was ~1.22 T, with similar field intensities of inflection for YbO and HoO containing glasses. One is reminded again, that in the single crystal sample of NaCl, no inflection was seen anywhere and no deviation from linearity could be observed.

In attempting to determine the origin of the kinks noted, the factors common to the different samples evidencing them must be considered. The semiconductor quantum dots represent a fairly well-controlled and fairly homogeneous experimental substrate, but the rare earth containing glasses do not. They are amorphous and inhomogeneous beyond a certain diameter. The quantum dots may have fairly consistent electronic properties, but those of the rare earth containing glasses may be less consistent. They do not have consistently and homogeneous potential barriers either. One possible unifying explanation for the phenomenon noted to occur in the above samples involves electron spins in a magnetic field.

The incident laser excites electrons from the valence to the conduction band, or from the highest occupied molecular orbital to the lowest unoccupied molecular orbital (if one uses the HOMO-LUMO terminology). Similarly, for the rare earth containing glasses, there are likely electrons which are excited by the incident laser radiation. We may then further hypothesize quantum dots or quantum dot-like regions (PBRs) have a small, but finite number of excited electrons, which behave as free electrons. The existence of such electrons, each with spins of $\pm\frac{1}{2}$ may give rise to combinations of spin with magnetic moments which are of interest. The following discussion follows from [77,78] by Holstein and Primakoff. A system with three interacting electrons will be subject to Coulombic and magnetic interactions. Evaluating first, the magnetic interactions between the magnetic moments of the electrons themselves, we have, for the magnetic correlation energy, U, between two electrons,

$$U = \frac{1}{r^3} [\mathbf{m}_1 \cdot \mathbf{m}_2 - 3(\mathbf{m}_1 \cdot \mathbf{n})(\mathbf{m}_2 \cdot \mathbf{n})] \quad (8.45)$$

Then, to an approximation,

$$U_{\text{dipole-dipole}} \approx \frac{1}{r^3} (m_1 m_2) \quad (8.46)$$

And, for $m_1, m_2 \sim g\mu_B \sim eh/m$ and $r \sim 2$ Angstroms, and μ_b as the Bohr magneton, we have,

$$U \sim \frac{(g\mu_B)^2}{r^3} \sim \left[\frac{e^2}{\hbar} \right]^2 \left(\frac{a_0}{r} \right)^3 \sim 10^{-4} \text{ eV} \quad (8.47)$$

Using kT , this represents a temperature of approximately 1K. Thus, such interactions could only be assessed in experiments using pumped liquid helium, and are too small to be entertained as a cause of the phenomena observed.

Next, we will assess the energy for one such electron magnetic moment in an externally applied magnetic field. Here, we note the energy will be,

$$\Delta E \sim g\mu_B BS \sim \mu_B B. \quad \mu_B = e\hbar / 2m \sim 5.8 \times 10^{-5} \text{ eV T}^{-1} \quad (8.48)$$

which for a 1 Tesla field is once again, $\sim 10^{-4}$ eV.

Now, a group of magnetic moments are treated differently from single magnetic moments, and the average magnetic moment, $\langle m \rangle$, is given by,

$$\langle m \rangle = g\mu_B \frac{1}{2} \frac{\left(e^{-\frac{1}{2}g\mu_B B / kT} - e^{+\frac{1}{2}g\mu_B B / kT} \right)}{\left(e^{-\frac{1}{2}g\mu_B B / kT} + e^{+\frac{1}{2}g\mu_B B / kT} \right)} = g \frac{\mu_B}{2} \tanh\left(\frac{\mu_B B}{kT} \right) \approx \mu_B \frac{\mu_B B}{kT} \quad (8.49)$$

so that the energy, $E \approx \frac{(\mu_B)^2 B^2}{kT}$ (8.50)

This, calculated, gives energy of approximately the same magnitude as the above equation and is thus too low to exceed the thermal background at room temperature.

Coulombic interactions play a part in the interaction of electron spins as well, and these interactions affect the total energies of a system with multiple interacting electrons. In our discussion of these effects, we will first look at Hund's rules. These rules are a consequence of a physical system's tendency to reduce its potential energy. In the first of these rules, the Coulombic interaction is minimized by the spatial part of the wave function for the two electrons being anti-symmetric. Here the node in the spatial part of the wave function keeps the electrons apart. In the second of these rules, the angular momentum quantum number, L , is maximized. Maximizing the angular momentum quantum number has the same effect as antisymmetrizing the spatial portion of the wavefunction. Namely, this minimizes the coulombic interaction. Maximizing the angular momentum, L , keeps the electrons spatially distant from each other. If we now recall,

$$E \sim \frac{(\mu_B)^2 B^2}{kT}, \tag{8.51}$$

then we can assess the energy for a group of correlated magnetic moments. Such correlated magnetic moments will be expected to produce an average total magnetic moment significantly greater than isolated moments. Then, if we call the range of this correlation to be ξ , then using

$$\frac{4\pi\xi^2}{3a^2},$$

the formula for the volume of a sphere, and a lattice spacing of a , we have, correlated magnetic moments. For $\xi/a = 4$, or four lattice spacing, we have, $\sim 2.7 \cdot 10^2$ moments correlated. Then, again using the above equation for the energy and for a field intensity of approximately 1.2 T, we have $\sim 400\text{K}$ as an effective temperature, and for a 2 T field, an effective temperature of $\sim 1000\text{K}$.

In the above discussion, no mention was made regarding exchange interactions between electrons. The exchange interaction between two electrons is dependent upon the concept of the in-distinguishability of the two electrons, allowing them to form quantum mechanical states, lowering their combined energies. Thus, the interactions become energetically favorable. Then, two $s = \frac{1}{2}$ electrons will have, for example, spins, $\uparrow 1, \downarrow 2$, the subscripts allowing us to distinguish between the two electrons. The Heisenberg Exchange Hamiltonian is then used,

$$H = 2J\sigma_1 \cdot \sigma_2 \tag{8.52}$$

where J is the exchange splitting between the two electrons. Here

$$\left\{ \begin{array}{l} |\uparrow\uparrow\rangle \\ |\uparrow\uparrow\rangle + |\downarrow\uparrow\rangle \\ |\downarrow\downarrow\rangle \end{array} \right\} E_t \quad \left\{ |\uparrow\downarrow\rangle - |\downarrow\uparrow\rangle \right\} E_s \quad E_s - E_t = J \tag{8.53}$$

Then, the issue at hand is to calculate J , which will give us the strength of the exchange interaction between the electrons. In an attempt to assess the energy of the exchange interaction, we now look at the exchange integral [36]. Here, the matrix element for the exchange interaction is given by

$$\langle \mathbf{k}', \mathbf{k} | V | \mathbf{k}', \mathbf{k} \rangle = \int \Psi_{\mathbf{k}'}^*(\mathbf{r}_1) \Psi_{\mathbf{k}}^*(\mathbf{r}_2) V(\mathbf{r}_1 - \mathbf{r}_2) \Psi_{\mathbf{k}'}(\mathbf{r}_2) \Psi_{\mathbf{k}}(\mathbf{r}_1) d^3r_1 d^3r_2 \tag{8.54}$$

Here, \mathbf{k}, \mathbf{k}' are the wave vectors before and after the spin-exchange occur. V is the potential operator, which goes as, $e^2 / (r_2 - r_1)$, e being the electronic charge. Plane wave electronic states, such as the ones which would be involved in the conduction band may be evaluated through

$$\langle \mathbf{k}', \mathbf{k} | V | \mathbf{k}', \mathbf{k} \rangle = \frac{1}{\Omega^2} \int e^{-i(\mathbf{k}' - \mathbf{k})(r_2 - r_1)} V(r_2 - r_1) d^3 r_1 d^3 r_2 \quad (8.55)$$

Here, Ω is a normalization volume. Given the previous definition for V , and with $n_k, n_{k'}$ being the numbers of electrons in the initial and final states we have,

$$E_{ex} = -\frac{1}{2} \frac{4\pi e^2}{\Omega} \sum_{k', k} \frac{n_k n_{k'}}{|\mathbf{k}' - \mathbf{k}|^2} \quad (8.56)$$

And, for the exchange energy per electron, we have Equation 5.10 equal to,

$$\frac{E_{ex}}{N} = -\frac{1}{2} \frac{4\pi e^2}{\Omega} \sum_{k', k} \frac{n_k n_{k'}}{|\mathbf{k}' - \mathbf{k}|^2} = -\frac{4\pi e^2}{2N} \frac{\Omega}{(2\pi)^6} \int d^3 k' d^3 k \frac{n_k n_{k'}}{|\mathbf{k}' - \mathbf{k}|^2} \quad (8.57)$$

where we have used dk^3, dk'^3 as volume elements, thus moving Ω from denominator to numerator, in order to maintain consistency in the units of length^{-3} . Then, taking $n_k, n_{k'}$ as unity, and performing the integration in the Fermi sphere, with the variables of integration being k/k_F [79], the exchange energy per electron becomes a constant, multiplied by e^2/k_F . Then we have [79],

$$\frac{E_x}{N} = -\frac{3}{4} e^2 \left(\frac{3\rho}{\pi} \right)^{1/3} \quad (8.58)$$

Then, if the density of electrons is taken as the density in a quantum dot of radius 1 nm.; and, if we multiply the right side of Equation 5.13 by $1/\epsilon$ the dielectric constant, as constant, as is customary (for CdS, CdSe, it is approximately 9.35 – 10.2), we have, for a 3 electron quantum dot, we are left with approximately 200 meV per electron.

For ferromagnetic systems, the interaction energy is approximately 160 meV per pair of electrons. This compares favorably with our rough calculation for the exchange energies.

It should be noted that without an exchange interaction, there will be an equal number of spin up and down states, without a predilection for either; thus resulting in no net magnetic moment. Once the spin exchange integral comes into play, there is an impetus for electrons to align with the same spin direction. It is possible, therefore, that in an applied magnetic field, the electrons would have a tendency to align in the field. The stronger the field, the greater that tendency. Note that for a quantum dot of larger size, that there will be a lower density of electrons if, say, three or five electrons on average are in the conduction band.

Thus, the factor, ρ will be lower for larger quantum dots, and the exchange energy per electron will therefore be lower. If this is the case, then it is further possible that a larger externally applied magnetic field would be necessary to provide the impetus to align the spins in larger quantum dots; thus causing the linear relationship between quantum dot size and the magnetic field intensity at which the kinks are seen, as is noted experimentally.

If electrons in PBRs are elevated through photonic excitation to free electrons, then they may participate in spin-exchange interactions. In this way they may have commonality with electrons in semiconductor quantum dots whose electrons have been excited from the valence to the conduction bands. If an odd number of electrons, say three or five, are in the excited state, then they would tend to be in the most energetically favorable configuration, such as the singlet state depicted in Equation 5.7. The presence of an externally applied magnetic field could then, at a given field intensity, cause a state change from the singlet to the triplet state, with spins aligned along the magnetic field. Recalling the discussion on Faraday rotation, this would provide additional electrons to interact with the circularly polarized light from which plane polarized light is decomposable. This would in turn increase the Faraday rotation in a given direction, thus increasing the overall Verdet constant.

The way in which confinement influences the magnetic field intensity at which the transition occurs is open to question. It may be a simple issue of the excited electrons being brought into closer physical proximity with each other, and thus influencing the spin exchange interaction, or some interplay between a Coulombic interaction (which would tend to keep the electrons apart to minimize potential energy) and a spin exchange interaction, which would increase as the electrons were brought closer together.

Conclusions

From measurements of Faraday rotation of II-VI quantum dots and rare earth containing glasses certain interesting phenomena were found. First, it was found that there was an inflection in the slope of optical rotation versus external magnetic field intensity. This appeared to be related to the size of the quantum dots, as for CdSe quantum dots of good homogeneity in both size and sphericity; there is a clear decrease in the point of inflection with decreasing dot size. The smallest of the CdSe dots, with a size of 1.1 nm, barely a few atoms in dimension, evidenced what appears to be two separate inflection points. It is theorized that the inflections are associated with energy transitions intrinsic to quantum confined systems but the glass properties involving intermediate range order also play a strong part in the non-linear behavior observed, especially in the rare-earth containing glass samples.

Whereas Faraday rotation curves are generally linear, as predicted by the classical derivation for the right and left rotatory indices of refraction; the experimental data demonstrated kinks in the optical rotation curves. These kinks were found also in borosilicate glass doped with rare earth elements. Subsequent work demonstrated the best fits for the plots were not polynomial, exponential, nor logarithmic curves, but were, indeed kink curves (or discontinuities) [38]. Significantly, these kinks were neither observed in the base glass, nor were they seen in NaCl salt crystals.

A variety of possible explanations were discussed for the observed kinks. While impurity levels could decrease (or increase) the bandgap energies, neither would explain the kinks seen.

Exciton confinement was noted to lower the bandgap energies, and exciton confinement in parallel arrays of quantum wells is believed to increase their Faraday rotation. However, as discussed above, exciton confinement as a cause of the effects seen has several difficulties. First, in the rare earth doped glasses, the regions of intermediate-range order can be expected to be highly irregular with many vertices. Such vertices cause piezoelectric charge build-up, and this effectively isolates electrons and holes, thus causing them to become uncorrelated. Furthermore, at the levels of confinement studied, the energies of confinement effectively uncorrelated the electrons and holes in any event, leaving them to behave as independent particles; and relegating the coulombic interaction between them to a perturbation.

The possible effects of Landau levels were examined as well. Here, it was determined that due to the high degree of electronic confinement, the formation of Landau levels would effectively violate one of the central postulates of quantum mechanics. Therefore they could not exist without the need to hypothesize huge fields of ~ 300 Tesla within the electron's orbit. And, if one did hypothesize a "tunneling" of the electron through a "magnetic barrier", one would be left with the prospect of a 300 Tesla field within a quantum dot. This would be expected to be observable through its effects on the other electrons in the quantum dot; and thus far, such changes in the absorption spectrum have not been observed. Thus, Landau levels were discounted as a possible cause of the effect seen.

Simple confinement energies were found to increase as inverse quadratic with respect to quantum dot size, whereas the kinks were found to demonstrate a linear relationship between quantum dot size and the magnetic field intensity at which the kinks were seen. Simple confinement was therefore discarded as a possible explanation.

The existence of impurity states would be expected to increase or decrease the bandgap energies, as discussed above. They would not, however, be expected to cause the kinks.

The 488 nm laser was quite close to the bandgap energy of the smallest of the CdSe quantum dots, and thus, a significant component of the high Verdet constants was undoubtedly due to a resonance effect. There were many other samples which were far enough away from resonance (0.5 – 1 eV), that resonance as a cause of the kinks was discarded as well.

The kinks exist as a point of commonality between the semiconductor quantum dots studied, and the rare earth doped glasses. The kinks, which demonstrated a linear relationship between dot size and magnetic field intensity, were seen at lower field intensities for the rare earth glasses than for the semiconductor quantum dots.

Interestingly, and as noted above, short range order has been suggested to exist in glasses, as evidence by Raman spectroscopy. Such short range order may be thought of as a region of structure in the midst of regions of lesser ordered structuring. The surrounding disordered regions produce a potential barrier which simulates the bounded potential region which is a quantum dot. It is through the potential barrier that both structures confine electrons and phonons.

If both structures confine electrons and phonons, which is believed to be their major physical characteristic, then we may look to this confinement as a source of the phenomena seen. As indicated above, it is possible that both structures confine several electrons (possibly three to five) which have been elevated through laser excitation, from the valence to the conduction band.

It is further postulated that these electrons may assume parallel or antiparallel states. The antiparallel state is energetically preferred in the absence of an externally applied magnetic field. In the presence of such a magnetic field, however, there is a tendency for the electron spins to align with the magnetic field. As indicated in the Discussion section, the spin exchange integral is calculable for free electrons, such as may be seen in electrons elevated from the valence to the conduction bands in semiconductors. Then, as seen in Equation 5.13, the exchange energy is directly proportional to the cube root of the electron density. This relationship gives an inverse linear relationship between the exchange energy and the size of the quantum dot. Thus, larger quantum dots will be expected to evidence lower exchange energies than smaller quantum dots. Given the decrease in exchange energy for larger quantum dots, larger magnetic field intensity may be required to cause a transition and align the spins; which would in turn cause a transition in the electron spin alignment to a parallel state. The increase in total numbers of electrons oriented in the same direction would then be expected to result in greater Faraday rotation, and a higher Verdet constant, for reasons discussed above in the Theory section.

It is interesting to note that [79] the case of exchange interactions in free electrons was discussed as a *special case*, involving a simplified system. At this time, however, with the experimental availability of confined nanostructures, the *special case* may be achievable in the laboratory; and the experimental results presented above may be reflective of the special phenomena discussed.

Then, as indicated in the theory section, this would allow a net increase in one of the two indices of refraction, n_+ or n_- . The increase results from an increase in the number of electrons of a single orientation, which can participate in spin transitions from $m = -\frac{1}{2}$ to $+\frac{1}{2}$, or vice versa. If this is the case, then it would be a process which could be common both to semiconductor quantum dots, as well as to potential-bounded regions in rare earth containing glasses. Once the spins begin alignment, the spin exchange energy becomes an impetus to continued electron spin alignment. It is this increased alignment which results both in increased magnetic moments; and which should result in higher Verdet constants for reasons described above.

It is interesting that the kinks in the rare earth containing glasses occur at significantly lower field intensities. This may be due in part to the amorphous nature of the potential-bounded regions. As seen in Figures 2 and 3 electrons are confined to areas in the quantum dot when there is significant charge build-up at sharp vertices. These are the sort of vertices which would be expected to be common in amorphous confined regions, such as might be seen in rare earth doped glasses. Please note in figure 3 the central location of the electrons in such confined regions; suggesting that physical regions in the amorphous potential bounded regions of rare earth doped glasses may be much smaller than the actual region itself. Thus, the confined region accessible to the electrons in such structures may be quite small indeed, and explain the lower field intensities at which the kinks are seen in these samples. Finally, let us compare some recent studies which may to some extent agree with our experimental observations. Savchuk, et. al. [84] studied the Magneto-optical faraday effect in II-VI based semimagnetic semiconductor nanocrystals at external magnetic fields up to 20 Tesla and at temperatures of 5K, however do not see any deviation from linearity in the Faraday rotation. This may give further credence that the intermediate order in our host glass may play a substantial part in the observed non-linearity in both of our groups of samples, namely the quantum dots and the rare earth containing glasses.

The Faraday Effect from Cobalt single-metal nano-particles was measured by J. Szczytko, et. al. [85] at external magnetic fields up to 0.4 Tesla and for five different wavelengths. The nanoparticles were contained in organic surfactants to prevent particle aggregation. Their work contains both theory and measurements. The measurements demonstrate nonlinearity in the form of a smooth curve around external field values from ~ 0.025 to 0.07 Tesla. The theoretical curves agree fairly well with their experimental data. Again their sample environment is different from our case since no intermediate range order exists and their external field range is a much lower value. An additional work also exhibits a non-linearity in the Faraday Effect from Bismuth-Telluride quantum dots/ quantum rods in glass [86]. Again their nonlinearities occur at much lower external magnetic field values than the range used in our work.

A magneto-optical study on ferric oxide quantum dots in a stable phosphate glass system by S. N. Garaje, et. al. [87] show changes in the Verdet constants which are quantum dot size dependent. Unfortunately, their external magnetic field is to a maximum of only 5.5 mTesla.

References

1. H.S. Bennett and E.A. Stern, *Phys. Rev.* **137**(2A) (1965), 448.
2. J. Kolodziejczak, B. Lax and Y. Nishina, *Phys. Rev.* **128**(6) (1962), 2655.
3. K. Suzuki and E. Hanamura, *J. Phys. Chem. Solids* **30** (1969), 749.
4. Y.I. Ukanov, *Sov. Phys. Usp.* **16**(2) (1974), 236.
5. Y. Nishina and B. Lax, *J. Phys. Chem. Solids* **30** (1969), 739.
6. R.B. Dennis, S.D. Smith and C.J. Summers, *Proc. Roy. Soc. Lond A* 321(1971), 303.
7. I.M. Boswarva, R.E. Howard and A.B. Lidiard, *Proc. Roy. Soc. Lond A* **269** (1962), 125
8. D.L. Mitchell and R.F. Wallis, *Phys. Rev.* **131**(5) (1963), 1965.
9. D.V. Bartholomew, J.K. Furdyna and A.K. Ramdas, *Phys. Rev. B* 34, 6943 (1986)
10. G. Chen, X.L. Yang, L. Zeng, J.X. Yang and F.F. Gong, *J. Appl. Phys.* 87(9), 5263 (2000)
11. M. Haddad, R. Andre', R. Frey and C. Flytzanis, *Solid State Commun.* 111,61 (1999).
12. Y. Wang, N. Harron, K. Moller and T. Bein, *Sol. State Com.* 77(1), 33 (1991).
13. A.K. Bhattacharjee, *Phys. Rev. B* 58(23), 15660 (1998).
14. A.I. Savchuk, I.D. Stolyarchuk, S.V. Medynskiy, A. Perrone and P.I. Nikitin, *Thin Solid Films* 336, 176 (1998).
15. J.A. Gupta, D.D. Awschalom, X. Peng and A.P. Alivisatos, *Phys. Rev. B* 59(16), R10 421 (1999).
16. P.I. Nikitin, et. Al. *Soviet J. of Quantum Electronics* 28(7), 561 (1998).
17. A. D. Buckingham and P.J. Stephens, *Magnetic Optical Activity*, Annual Reviews, 1965, www.annualreviews.org/online.
18. P.J. Stephens, *Theoretical Studies of Magneto-optical Phenomena* (Doctoral Thesis, Oxford Univ., Oxford 1964)
19. D.B. Hall, K. Vogel, J. Schroeder, *J. of Physics: Condensed Matter* **10**(26), 6009 (1998).
20. W. Kauzmann, *Quantum Chemistry*, Chaps. 15, 16 (Academic Press, New York, 1957)
21. Yu. I. Ukhanov, *Usp. Fiz. Nauk.* **109** 667-694 (April, 1973).
22. G. W. Bryant, *Excitons in Zero-Dimensional Nanostructures*, in *Optics of Excitons in Confined Systems*, 131-138, *Inst. of Physics Conf. Ser. No. 123*, September, 1991.
23. A. Filin, Dept. of Physics, Rensselaer Polytechnic Institute, unpublished material.
24. P.D. Persans, M. Silvestri, G. Mei, E. Lu, H. Yukselici and J. Schroeder, *Brazilian J. of Physics* **23**2 (1993), 144.
25. K. Nakamura and H. Nakano, *J. of Physical Soc. of Japan*, **61** (4) (1992), 1390.
26. G. Bastard, E.E. Mendez, L.L. Chang and L. Esaki, *P. Rev. B.* **15**(1982), 1974.
27. G. Gourdon, G. Lazard, V. Jeudy, C. Testelin, E.L. Ivchdenko and G. Karczewski, *Solid State Commun.* **123**, (2002), 299.
28. S.D. Smith, *Optical Properties of Solids: Magneto-optics*, eds. S. Nudelman and S.S. Mitra, (New York, Plenum) (1969), 85.
29. G.R. Fowles, *Introduction to Modern Optics* (New York, Holt, Reinhart and Winston (1968), 189.
30. J.G. Mavroides, *Optical Properties of Solids: Magneto-optical Properties*, ed. F.

- Abeles (Amsterdam, N. Holland) (1972), 364.
31. E.U. Condon, *Rev. Mod. Phys.* **9** (1937), 432.
 32. A. Sommerfeld, *Optics* (New York, Academic) (1954), 101.
 33. H.R. Hulme, *Proc. R. Soc.* **135** (1935), 237.
 34. J.H. Van Vleck, *Phys. Rev.* **46** (1934), 17.
 35. J.H. Van Vleck, *The Theory of Electric and Magnetic Susceptibilities*, Oxford University Press (1932).
 36. Y.J. Yu and R.K. Osborn, *Phys. Rev. A* **15** (1977), 2404.
 37. E. Yu. Perlin, *Optics and Spectroscopy* **88**(6) (2000), 898.
 38. J.H. Kratzer and J. Schroeder, *J. Non-Crystalline Solids*, **349** (2004), 299.
 39. G. W. Scherer, *J. Non-Cryst. Solids* **123**, 75 (1990).
 40. C. T. Moynihan, P.B. Macedo, C.J. Montrose, P.K. Gupta, M.A. DeBolt, J.F. Dill B.E. Dom, P.W. Drake, A.J. Easteal, P. Elterman, R. P. Moeller, H. Sasabe, and J. Wilder, *Ann. NY Acad. Sci.* **279**, 15 (1976).
 41. C.T. Moynihan and J. Schroeder, *J. Non-Cryst. Solids* **160**, 52 (1993).
 42. G. Adam and J. H. Gibbs, *J. Chem. Phys.* **43**, 139 (1965).
 43. U. Mohanty, *Physica A* **177**, 345 (1991).
 44. U. Mohanty, *J. Chem. Phys.* **100**, 5905 (1994).
 45. C.A. Angell, C.T. Moynihan and M. Hemmati, *J. Non-Cryst. Solids* **274**, 319
 46. L. D. Landau and E. M. Lifshitz, *Statistical Physics* (Addison-Wesley, Reading, MA, 1969) pp. 343-354.
 47. R.E. Robertson, *J. Polym. Sci.: Pol. Sym.* **68**, 173 (1978); and R.E. Robertson, *J. Polym. Sci.: Pol. Sym.* **69**, 597 (1979).
 48. I. M. Hodge, *Macromolecules* **20**, 2897 (1987); *J. Non-Cryst. Solids* **131-133**, 435 (1991).
 49. M. H. Cohen and G. S. Grest, *Phys. Rev. B* **24**, 4091 (1981); M. H. Cohen and D. Turnbull, *J. Chem. Phys.* **31**, 1164 (1959).
 50. P.K. Dixon and S.R. Nagel, *Phys. Rev. Lett.* **61**, 341 (1998)
 51. N. Menon, S. R. Nagel and D.C. Venarus, *Phys. Rev. Lett.* **73**, 963 (1994).
 52. J. Schroeder, Light scattering of glass in *Treatise on Material Science and Technology*, **12**, ed. M. Tomozawa and R. H. Doremus, (Academic Press, New York, 1977), pp.157-222.
 53. H.A. Cummins, *Proceedings of the International School of Physics*, ed. R.J. Glauber (Academic Press, New York, 1969), pg. 247.
 54. R. Shuker and R. W. Gammon, *Phys. Rev. Lett.* **25**, 222 (1970).
 55. R. Shuker and R. W. Gammon, Light scattering in Solids, in *Proceedings of Second International Conference*, ed. M. Balkanski, (Flammarion Sciences, Paris, 1971), pp.334-338.
 56. J. Jäckle, Low frequency Raman scattering in glasses, in *Amorphous Solids-Low Temperature Properties*, ed. W. A. Phillips, (Springer-Verlag, Berlin, 1981), pp. 135-160.
 57. A. P. Sokolov, A. Kisliuk, M. Soltwisch and D. Quitmann, *Phys. Rev. Lett.* **69**, 1540 (1992).
 58. V. K. Malinovsky, V.N. Novikov, P.P. Parshin, A.P. Sokolov and M.G. Zemlyanov, *Europhys. Lett.* **11**, 43 (1990)
 59. A. Fontana, F. Rocca, M.P. Fontana, B. Rosi and A.J. Dianoux, *Phys. Rev. B* **41**, 3778 (1990).

60. A. P. Sokolov, A. Kisliuk, D. Quitmann and E. Duval, Phys. Rev. B **48** (10), 7692 (1993).
61. J. Wuttke, J. Hernandez, G. Li, G. Coddens, H.Z. Cummins, F. Fujara, W. Petry and H. Sillescu Phys. Rev. Lett. **72**, 3052 (1994).
62. G. Carini, G. D'Angelo, G. Tripodo, A. Fontana, A. Leonardi, G.A. Saunders and Brodin, Phys. Rev. B **52**, 9342 (1995).
63. C. Levelut, N. Gaimes, F. Terki, G. Cohen-Solal, J. Pelous and R. Vacher, Phys. Rev. B **51** (13), 8606 (1995).
64. D. Quitmann, M. Soltwisch, and G. Ruocco, J. Non-Cryst. Solids **203** 12-18 (1996).
65. O. Yamamuro, I. Tsukushi, and T. Matsuo, J. Chem. Phys. **106**, 2997 (1996).
66. M. T. Dove, M. J. Harris, A.C. Hannon, J.M. Parker, I.P. Swainson and M. Gambhir, Phys. Rev. Lett. **78**, 1070 (1997).
67. A. Fontana, F. Rossi, G. Carini, G. D'Angelo, G. Tripodo and A. Bartolotta, Phys. Rev. Lett. **78** (6), 1078 (1997).
68. A. F. Ioffe and A. R. Regel, Prog. Semicond. **4**, 237 (1960).
69. N.F. Mott, Conduction in Non-Crystalline Materials (Clarendon Press, Oxford, 1987), pp. 5,22,92.
70. W. Schirmacher and H. Wagner, Springer Proc. Phys. **37**, 231 (1989).
71. J.H. Kratzer, "Magneto-Optic Properties of II-VI Semiconductor Quantum Dots", Ph.D. Dissertation, Rensselaer Polytechnic Institute, Troy, NY, May, 2005.
72. J.M. Ziman, Theory of Solids (London, Cambridge University Press) (1964).
73. R. Dutt and A. Mukherjee, Phys. Rev. A **52**(3) (1995), 1750.
74. T. Sako, and G.H.F. Diercksen, J of Physics B: At. Mol. Opt. Phys. **36** (2003), 1681.
75. J.Schroeder, J.H.Kratzer and J.L. Apkarian, Phys.Chem of Glasses: Eur. J. Glass Sci. Technol.B. **49**(6) (2008), 305.
76. J. Schroeder, M. Lee, L-G. Hwa and C.T. Moynihan, "Nanoscale Inhomogeneities and Order In Glasses" in Encyclopedia of Nanoscience and Nanotechnology: Ed. H.S. Nalwa, **18** (2011), 365.
77. T.Holstein and H.Primakoff, Phys. Rev. **58**(1940) 1098
78. T. Holstein and H. Primakoff, Phys. Rev. **59** (1941), 388.
79. W. Harrison, "Solid State Theory", Dover Publication, New York 1979.
80. V. K.Malinovsky and A.P. Sokolov, Solid State Communications, **57**(9), (1986) 757.
81. S.R.Elliot, Europhys. Letters, **19**, (1992) 201.
82. P.Benassi, et. Al., Philos. Mag., **B71**, Fourth Edition, (1995) 761.
83. J.Schroeder and J.H.Kratzer, J. Non-crystalline Solids, **358**, (2012), 3517.
84. A. I. Savchuk, et. al., Phys. Stat. Sol. (c), **3** (4), (2006), 1160.
85. J. Szczytko, et. al. Phys. Rev. E **87**, (2913), 033291.
86. R. P. Panmand, et. al. Phys. Chem. Chem. Phys., **14**, (2012), 16236.
87. S. N. Garaje, et. al.; Materials Research Bulletin, (**48**), (2013), 901.